

Design, Synthesis, and Biological Evaluation of [1,2,5]Oxadiazolo[3,4-*b*]pyridin-7-ol as Mitochondrial Uncouplers for the Treatment of Obesity and Metabolic Dysfunction-Associated Steatohepatitis

Mary A. Foutz, Emily L. Krinos, Martina Beretta, Stefan R. Hargett, Riya Shrestha, Jacob H. Murray, Ethan Duerre, Joseph M. Salamoun, Katrina McCarter, Divya P. Shah, Kyle L. Hoehn,* and Webster L. Santos*



Cite This: *J. Med. Chem.* 2024, 67, 21486–21504



Read Online

ACCESS |



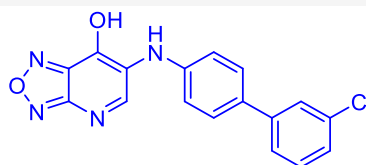
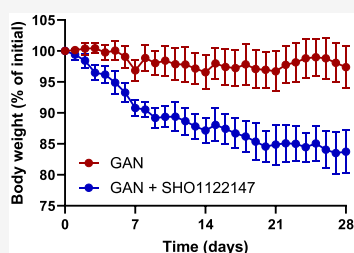
Metrics & More



Article Recommendations



Supporting Information



SHO1122147 (7m)

EC₅₀ = 3.6 μM

t_{1/2} = 2.0 h

C_{max} = 35 μM

- potent and efficacious mitochondrial uncoupler
- reduces body weight without impacting lean mass
- improves MALFD activity score

ABSTRACT: Mitochondrial uncouplers are small molecule protonophores that act to dissipate the proton motive force independent of adenosine triphosphate (ATP) synthase. Mitochondrial uncouplers such as BAM15 increase respiration and energy expenditure and have potential in treating a variety of metabolic diseases. In this study, we disclose the structure–activity relationship profile of 6-substituted [1,2,5]oxadiazolo[3,4-*b*]pyridin-7-ol derivatives of BAM15. Utilizing an oxygen consumption rate assay as a measure of increased cellular respiration, SHO1122147 (7m) displayed an EC₅₀ of 3.6 μM in L6 myoblasts. Pharmacokinetic studies indicated a half-life of 2 h, C_{max} of 35 μM, and no observed adverse effects at 1,000 mg kg⁻¹ dose in mice. In a Gubra-Amylin (GAN) mouse model of MASH, SHO1122147 was efficacious in decreasing body weight and liver triglyceride levels at 200 mg kg⁻¹ day⁻¹ without changes in body temperature. These findings indicate the potential of utilizing novel [1,2,5]oxadiazolo[3,4-*b*]pyridin-7-ol mitochondrial uncouplers for treatment of fatty liver disease and obesity.

INTRODUCTION

Obesity affects 42% of people in the United States and is defined as an accumulation of excess body fat as a result of a higher influx of calories versus energy expended.¹ Obesity is a chronic disease with multiple comorbidities including cardiovascular disease,² type 2 diabetes,³ and nonalcoholic fatty liver disease.⁴ The disease can place excess stress on joints and drastically impact a patient's physical activity.⁵ Not only is quality of life severely impacted, but in the United States alone, the yearly medical cost of obesity is estimated to be \$173 billion.⁶

Obesity is defined by having a body mass index (BMI) score of 30 or above. Reducing caloric intake and increasing exercise are the primary means of maintaining a BMI in a healthy range. However, patient compliance with lifelong voluntary food restriction or exercise is poor, which makes healthy weight maintenance challenging.⁷ An effective treatment option is bariatric surgery; however, the procedure is not a global solution due to high cost and risk.⁸

In contrast, pharmaceutical treatments with low adverse effects represent a solution with potential high compliance. The glucagon-like peptide 1 (GLP-1) receptor agonist semaglutide is an injectable treatment for type-2 diabetes.⁹ It was approved by the FDA for weight loss in 2021, quickly becoming a popular option for obesity treatment as it leads to decreased appetite and food intake.¹⁰ In 2023, the FDA also approved tirzepatide for weight loss. Tirzepatide activates both GLP-1 and glucose dependent insulinotropic polypeptide (GIP).^{11,12} While both treatments are effective, undesirable side effects such as adverse gastrointestinal complications, including moderate to severe diarrhea, nausea and vomiting are

Received: October 1, 2024

Revised: November 14, 2024

Accepted: November 21, 2024

Published: November 30, 2024



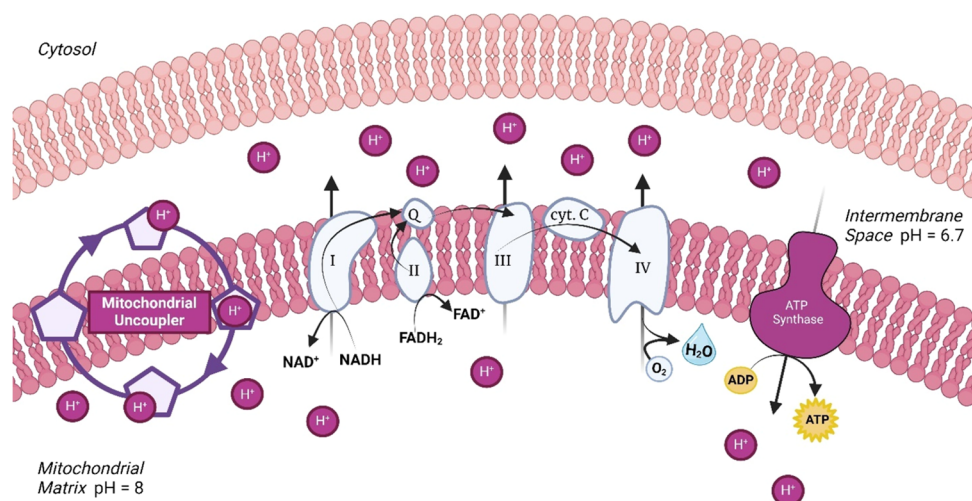


Figure 1. Electron transport chain established the proton motive force while mitochondrial uncouplers facilitates a “proton leak”.⁴³

observed.¹³ In STEP-1 clinical trials, semaglutide resulted in up to 40% loss of lean mass.¹⁴ Semaglutide and tirzepatide also have a boxed warning for increased risk of medullary thyroid carcinoma and are linked to a risk of optic nonarthritic anterior ischemic neuropathy.¹⁵ Subsequently, there is significant opportunity to develop new drugs that do not decrease lean mass or cause debilitating adverse effects.

While obesity is still an overwhelming problem worldwide, the number and availability of treatment options are increasing. However, when in conjunction with comorbidities such as metabolic dysfunction-associated steatohepatitis (MASH), treatment plans become exceptionally limited.¹⁶ MASH is an advanced form of metabolic-dysfunction associated fatty liver disease (MAFLD) where early stage liver injury progresses to steatosis and liver inflammation that can eventually lead to cirrhosis and hepatocellular carcinoma.^{17–19} To date, MASH has only one FDA-approved pharmaceutical: resmetirom—a liver-targeted thyroid hormone receptor- β agonist.²⁰ Beyond this treatment, liver transplantation is the only other option. However, obesity puts patients at a higher risk for the recurrence of liver disease following transplantation.^{21,22} Thus, finding therapies to treat MASH and reverse obesity would be extremely beneficial.

While the etiology of MASH is unknown, the progression of the disease can be attributed to production of reactive oxygen species (ROS) leading to a necro-inflammatory environment.^{23–25} Similarly, obesity is a low-grade inflammatory disease that has been linked to high levels of reactive oxygen species in adipose tissue causing oxidative stress and mitochondrial dysfunction.²⁶ Beyond GLP-1 and thyroid hormone receptor- β agonists, innovative strategies geared toward reducing mitochondrial dysfunction are being explored. Specifically, mitochondrial uncouplers are of interest for the treatment of both MASH and obesity because they act as “fat-burning” molecules that reduce ROS production at their source.

Mitochondrial oxidative phosphorylation is used for approximately 95% of adenosine triphosphate (ATP) synthesis in most cells (Figure 1).²⁷ In noninjured cells, mitochondria convert nutrients into ATP through a process that involves a proton cycle across the mitochondrial intermembrane. Nutrient oxidation in the mitochondrial matrix results in the efflux of protons into the mitochondrial intermembrane space

creating a proton motive force (PMF). The resulting electrochemical gradient drives ATP synthesis as protons re-enter the matrix via ATP synthase. During this metabolic process, electrons leak from electron transport chain complexes I and III where they react with molecular oxygen to form ROS, causing inflammation.^{23,24,28} Uncoupling proteins (UCPs) induce mitochondrial uncoupling—a process where protons are transported into the matrix independent of ATP synthase, causing an increase in respiration.²⁹ Efficient respiration facilitates low residence time of electrons in complex I and III, leading to a reduction of ROS formation. Thus, mitochondrial uncoupling as a potential treatment strategy for both obesity and MASH.

Unfortunately, UCPs are considered undruggable targets due to their closed activation site.³⁰ However, small molecules that act as proton shuttles can be utilized as alternatives to UCPs. 2,4-Dinitrophenol (DNP) was the first small molecule mitochondrial uncoupler reported where weight loss was first observed (Figure 2).³¹ However, DNP was banned by the

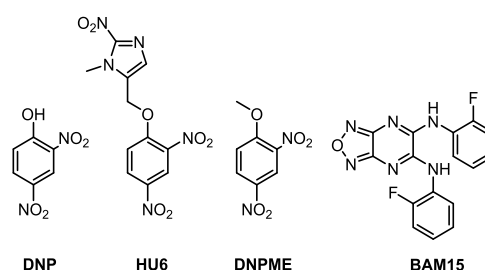


Figure 2. Chemical structures of select small molecule mitochondrial uncouplers.

FDA due to severe side effects such as hyperthermia, blindness, and even death.^{31–34} DNP has a narrow therapeutic window and is linked to off-target effects including depolarizing the plasma membrane and increasing intracellular calcium.^{35,36} To mitigate these issues, DNP prodrugs including liquid crystal gel (DNP LC-Gel), DNP methyl ether (DNPME), and extended release (CRMP) formulations are being explored for treatments of diabetes and MASH. Most recently, prodrug HU6 is undergoing phase II clinical trials for the treatment of MASH.^{37–42}

Our lab has an ongoing interest in small molecule mitochondrial uncouplers that are structurally distinct from DNP. In 2014, we discovered BAM15 as a mitochondrial selective uncoupler.⁴⁴ Since then, BAM15 has shown promise as a therapeutic agent for diseases such as cancer, diabetes, obesity, MASH, and sepsis.^{45,46}

Using the BAM15 scaffold as a prototype, second generation analogs were developed (Figure 3).⁴⁷ By substituting one of

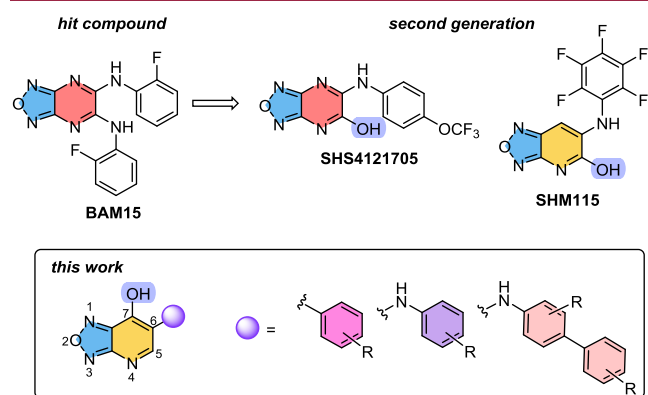


Figure 3. Past and current work on structure–activity relationship studies of BAM15.

BAM15's aniline groups for a hydroxy moiety, compounds with improved properties were discovered. Specifically, to optimize the pyrazine core, structural evolution to a pyridine core generated SHM115, which had greater distribution in white and brown adipose tissues and was efficacious for the treatment of Western diet induced obesity in mice.⁴⁸ While

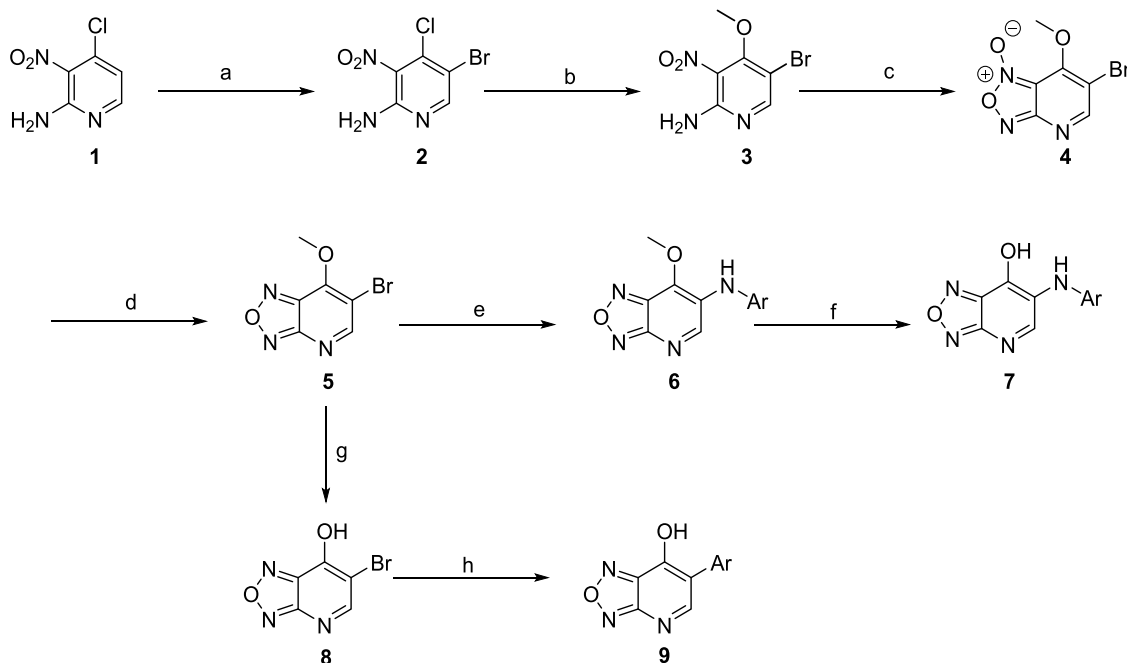
maintaining the pyrazine core of BAM15 and incorporating a hydroxy group, lead compound SHS4121705 was revealed with a half-life of 5.7 h in mice. SHS4121705 was primarily localized in the liver and was efficacious in a STAM mouse model of MASH.⁴⁷ However, the STAM model is a chemically induced process that does not accurately mimic human MASH pathology.^{49,50} Thus, in this study, a more clinically relevant MASH-mouse model was employed.

In a continued effort to optimize the BAM15 scaffold, a new generation of mitochondrial uncouplers is described. The key transformation is the transposition of the hydroxy group from the 5 to 7-position (Figure 3). We hypothesized that the pyridine core would mimic the lipophilicity of SHM115 and changing the hydroxy position could lead to enhanced potency while maintaining desirable pharmacokinetic properties. In this report, we installed unique aniline, biphenyl aniline, and phenyl groups onto the scaffold, then investigated their activity *in vitro* and *in vivo*. Our studies identified SHO1122147 as a potent uncoupler with an EC₅₀ of 3.6 μM. Additionally, it acts as an antiobesity and anti-MASH agent as determined by a more clinically relevant model of MASH, Gubra-Amylin NASH (GAN).

RESULTS

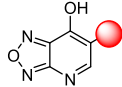
In this work, we aimed to investigate the synthetic route for the 6-(phenylamino)-[1,2,5]oxadiazolo[3,4-*b*]pyridin-7-ol derivatives with biphenyl aniline and phenyl substitution in the 7-position (Scheme 1). (7) began with commercially available 4-chloro-3-nitropyridin-2-amine **1**. Bromination with *N*-bromosuccinimide affords aniline **2** in good yield (83%). Nucleophilic aromatic substitution with sodium methoxide resulted in the

Scheme 1. Synthetic Route for the 6-(Phenylamino)-[1,2,5]oxadiazolo[3,4-*b*]pyridin-7-ol Derivatives with Biphenyl Aniline and Phenyl Substitution in the 7-Position^a



^aReagents and conditions: (a) *N*-bromosuccinimide, acetonitrile, 80 °C, 1 h, 83%; (b) sodium methoxide, methanol, 35 °C, 16 h, 80%; (c) (diacetoxyiodo)benzene, acetonitrile, 80 °C, 1 h, 77%; (d) triphenylphosphine, CH₂Cl₂, 40 °C, 16 h, 75%; (e) Pd₂(dba)₃, Xantphos, K₂CO₃, aniline, toluene, 110 °C, 8 h; (f) Na₂CO₃, 1,4-dioxane, water (2:1), 110 °C, 4 h, 8–82% yield over two steps; (g) KOH, water, 1,4-dioxane, rt, 15 min; (h) Pd(dppf)Cl₂·CH₂Cl₂, Ar–B(OH)₂, Na₂CO₃, 1,4-dioxane, water, 90 °C, 18 h, 7–34% yield over two steps.

Table 1. OCR Data of 6-Substituted Oxadiazolopyridine Derivatives



| Entry | R | % of BAM15 OCR ^a | EC ₅₀ , μM | Entry | R | % of BAM15 OCR ^a | EC ₅₀ , μM |
|-------|---|-----------------------------|-----------------------|-------|---|-----------------------------|-----------------------|
| BAM15 | - | Maximum Capacity | 0.31 ± 0.06 | 7j | | NA | NA |
| 7a | | 40 | 59 ± 3.4 | 7k | | NA | NA |
| 7b | | 38 | 49 | 7l | | NA | NA |
| 7c | | 50 | 14 ± 1.7 | 7m | | 69 | 32 ± 1.8 |
| 7d | | 19 | 1.0 ± 0.1 | 7n | | 55 | 51 ± 2.6 |
| 7e | | 7 | 2 ± 0.4 | 7o | | 32 | >100 |
| 7f | | 20 | 6.0 ± 0 | 7p | | 69 | 27 ± 1.9 |
| 7g | | 10 | >100 | 7q | | 57 | 34 ± 4.0 |
| 7h | | 38 | 6 ± 0.4 | 7r | | 48 | 22 ± 1.8 |
| 7i | | NA | NA | 7s | | 43 | 35 ± 1.7 |

^aRatio of integrated area under OCR dose curve above baseline relative to that of BAM15 from the same experiment expressed as percent. NA = No Activity. Highest tested concentration is 200 μM. BAM15 was tested up to 200 μM.

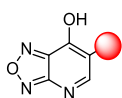
formation of the 3-bromo-4-methoxy-substituted pyridine intermediate **3**, which was followed by cyclization to form the furoxan **4** using (diacetoxyiodo)benzene. Reduction of the furoxan ring by triphenylphosphine generated 6-bromo furazanopyridine intermediate **5**. Buchwald-Hartwig cross-coupling reactions between anilines, intermediate **5**, and subsequent deprotection with K₂CO₃ in dioxane/water afforded the desired product **7**, 7-hydroxyoxadiazolopyridine. Alternatively, phenyl substituted derivatives (**9**) were synthesized from 6-bromo-7-methoxy-[1,2,5]oxadiazolo[3,4-*b*]pyridine (**5**) by deprotecting the methoxy group with potassium hydroxide to yield **8**. A Pd-catalyzed Suzuki-Miyaura coupling reaction generated various phenyl derivatives (**9**).

With **7** and **9** derivatives in hand, we screened for mitochondrial uncoupling activity as a function of oxygen consumption rate (OCR). OCR increases when a mitochondrial uncoupler transports protons across the intermembrane

of the mitochondria to the matrix, allowing the cell to increase respiration. Thus, increased respiration is detected by OCR. L6 rat myoblasts were treated with compounds for 90 min and subsequently analyzed on an Agilent Seahorse XF instrument (All compounds tested were >95% pure by UPLC analysis). Experiments were conducted at 8 different concentrations (0.37, 1.1, 3.3, 10, 25, 50, 100, and 200 μM) over the course of 200 min. Because OCR results are influenced by both cell density and quality, BAM15 was used as both as a positive control and standard for maximum OCR. OCR data was normalized by comparing area under the curve relative to BAM15. The minimum threshold for uncoupler properties includes an EC₅₀ value <5 μM and an OCR value >35% of BAM15.

The structure–activity relationship study (SAR) began by investigating an aniline (**7a**) to determine base activity (Table 1). While active as an uncoupler, a significant drop in both

Table 2. OCR Data of Multi-Substituted Aniline Derivatives



| Entry | R | % of BAM15 OCR ^a | EC ₅₀ , μM | Entry | R | % of BAM15 OCR ^a | EC ₅₀ , μM |
|-------|---|-----------------------------|-----------------------|-------|---|-----------------------------|-----------------------|
| 7t | | 60 | 64 ± 3.3 | 7aa | | 68 | 32 ± 1.9 |
| 7u | | 83 | 40 ± 1.9 | 7ab | | 71 | 43 ± 5.2 |
| 7v | | 69 | 64 ± 5.3 | 7ac | | 55 | 11 ± 6.7 |
| 7w | | 54 | 52 ± 8.8 | 7ad | | 55 | 28 ± 3.9 |
| 7x | | 55 | 63 ± 3.7 | 7ae | | 48 | 40 ± 4.5 |
| 7y | | 68 | 44 ± 3.6 | 7af | | 54 | 25 ± 12 |
| 7z | | 50 | 18 ± 2.4 | 7ag | | 38 | 40 ± 0.9 |

^aRatio of integrated area under OCR dose curve above baseline relative to that of BAM15 from the same experiment expressed as percent. NA = No Activity. Highest tested concentration is 200 μM. BAM15 was tested up to 200 μM.

efficacy and potency was observed (40%, 59 μM) when compared with BAM15. Further functionalization of the aniline allowed for tuning of the lipophilicity and acidity of the scaffold. Thus, an array of alkyl substituents in the *para* position (7b–7e) were synthesized and all but *t*-butyl aniline (7e) were tolerated. The most promising compound was the *para*-substituted ethyl tail 7c, with 50% of BAM15 OCR and an EC₅₀ of 14 μM. Unfortunately, alkyl-substituted analogs were found to have short half-life values in mice so further investigation of this series was not pursued (data not shown). An electron donating *t*-butyl ether analog (7f) had poor activity with only 20% BAM15. Several strong withdrawing groups (7i–7j) were then added in the *para* position. The only tolerated group was -SCF₃ (7h) but again its activity was reduced. The 3-aminopyridine analogs 7k and 7l were also inactive.

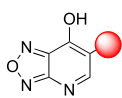
Inspired by previous work, halogen substituents were added in the *ortho*, *meta*, and *para* positions to identify the most optimal position.⁴⁸ The *ortho*-fluorinated 7m exhibited 69% of BAM15 uncoupling capability, a 72% increase when compared with the nonsubstituted aniline. However, fluorine substitution in the *meta* (7n) and *para* positions (7o) both decreased the OCR activity (55 and 32%, respectively). Substitution of the *ortho*-fluoro group for a chloro group (7p) resulted in improved EC₅₀ (27 μM), suggesting that the *ortho*-chloro

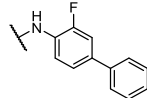
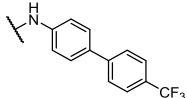
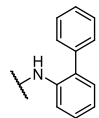
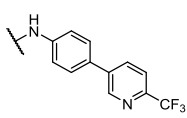
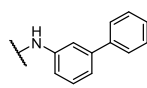
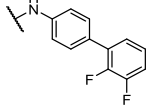
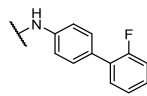
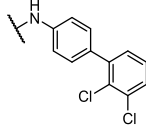
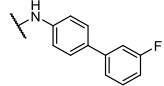
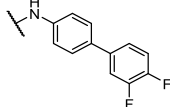
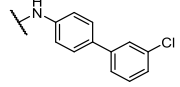
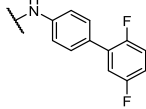
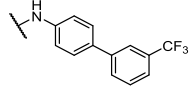
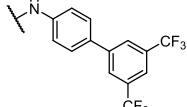
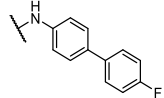
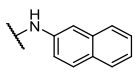
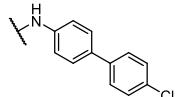
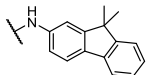
group increases potency. Use of the strongly electron withdrawing trifluoromethyl group in the *ortho*, *meta*, and *para* positions (7q–7s) was equally effective.

With the promising results from the monosubstituted aniline derivatives, multisubstituted analogs were investigated with fluorine in the *ortho* position (Table 2). All the difluoro-substituted aniline derivatives (7t–7w) had OCR values of >50% that of BAM15. However, the EC₅₀ values remained high (>40 μM). Additional fluorine atoms resulted in a successive improvement, but pentafluoroaniline 7z was the most potent. The 2-fluoro-3-chloro analog 7aa was also relatively potent at 32 μM. When a trifluoromethyl group was placed around the ring instead of chlorine in compounds 7ab, 7ac, and 7ad the potency improved with derivative 7ac having an EC₅₀ of 11 μM. Other variations did not significantly improve activity (7ae–7ag).

We next investigated the effect of the addition of an aryl ring to the aniline moiety (Table 3). 2-Fluoro-4-phenyl aniline 7ah showed limited OCR activity (10%). We then tested OCR for 2- and 3- phenyl anilines (7ai, 7aj) but neither were tolerated. Unfortunately, we were unsuccessful at synthesizing the 4-phenyl aniline analog. Next, we investigated the effect of substitutions on the pendant ring. First, the 2'-fluoro analog 7ak was not tolerated. This was followed by the *meta*-fluoro (7al), *meta*-chloro (7am), and *meta*-trifluoromethyl (7n)

Table 3. OCR Data of 4-[Phenyl]aniline Derivatives



| Entry | R | % of BAM15 OCR ^a | EC ₅₀ , μM | Entry | R | % of BAM15 OCR ^a | EC ₅₀ , μM |
|-----------------|-------------------------------------------------------------------------------------|-----------------------------|-----------------------|-------|--------------------------------------------------------------------------------------|-----------------------------|-----------------------|
| 7ah |  | 10 | 2.0 ± 0.5 | 7aq |  | NA | NA |
| 7ai |  | NA | NA | 7ar |  | 17 | 7.0 ± 1.9 |
| 7aj |  | 20 | 6.0 ± 1.2 | 7as |  | NA | NA |
| 7ak |  | NA | NA | 7at |  | NA | NA |
| 7al |  | 36 | 1.2 ± 0.1 | 7au |  | NA | NA |
| SHO1122147 (7m) |  | 55 | 3.6 ± 0.1 | 7av |  | NA | NA |
| 7an |  | 25 | 0.5 ± 0.1 | 7aw |  | 20 | 41 ± 4.9 |
| 7ao |  | 60 | 1.7 ± 0.2 | 7ax |  | 48 | 13 ± 1.2 |
| 7ap |  | 57 | 0.9 ± 0.1 | 7ay |  | NA | NA |

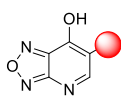
^aRatio of integrated area under OCR dose curve above baseline relative to that of BAM15 from the same experiment expressed as percent. NA = No Activity. Highest tested concentration was 200 μM. BAM15 was tested up to 200 μM.

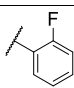
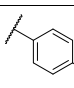
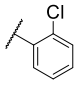
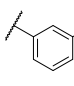
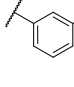
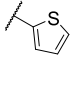
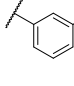
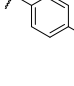
moieties. In this series we observe a significant improvement in both efficacy and potency, with **7al** and **7am** having EC₅₀ values of 1.2 and 3.6 μM, respectively. It was noted that the (**7an**) showed cellular toxicity at higher concentrations. Interestingly, when fluorine (**7ao**) or chlorine (**7ap**) atoms were placed on the 4' position, the activity of the compounds were not only in the low μM regime, but now possess favorable (<50%) OCR activity relative to BAM15. However, the 4'-

trifluoromethoxy analog **7aq** exhibited toxicity and was not tolerated. Unfortunately, further structural changes with pyridyl trifluoromethyl groups or disubstitution with halogens (**7ar**–**7aw**) resulted in decreased activity. Likewise, introducing fused ring systems in **7ax** and **7ay** also did not improve activity.

We next turned our attention to 6-phenyloxadiazolopyridine analogs where the aniline NH was removed. As shown in Table

Table 4. OCR Data of 6-Phenyl Oxadiazolopyridine Analogs



| Entry | R | % of BAM15 OCR ^a | EC ₅₀ , μM | Entry | R | % of BAM15 OCR ^a | EC ₅₀ , μM |
|-------|-----------------------------------------------------------------------------------|-----------------------------|-----------------------|-------|-----------------------------------------------------------------------------------|-----------------------------|-----------------------|
| 9a |  | 69 | 27 ± 2.8 | 9e |  | 52 | 12 ± 0.6 |
| 9b |  | 49 | 85 ± 16 | 9f |  | 37 | 15 ± 2.5 |
| 9c |  | 61 | 25 ± 3.1 | 9g |  | 36 | 40 ± 0.3 |
| 9d |  | 59 | 26 ± 4.5 | 9h |  | NA | NA |

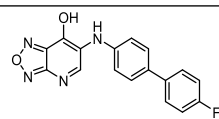
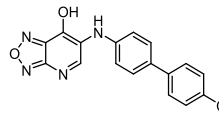
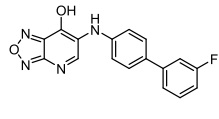
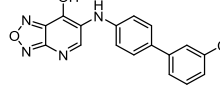
^aRatio of integrated area under OCR dose curve above baseline relative to that of BAM15 from the same experiment expressed as percent. NA = No Activity. Highest tested concentration is 200 μM. BAM15 was tested up to 200 μM.

4, 2-fluorophenyl analog (9a) had an EC₅₀ of 27 μM and 69% BAM15 activity. The chlorinated surrogate (9b) was less potent but moving the chlorine atom to the *meta* (9c) and *para* (9e) positions resulted in progressive improvement in potency with compound 9e having an EC₅₀ of 12 μM and 52% BAM15 activity.

Trifluoromethyl and trifluoromethoxy substituted derivatives 9d and 9f, while active, exhibited cellular toxicity at higher concentrations (data not shown). An analog with a heterocyclic group such as thiophene (9g) showed poor activity. Finally, a 4'-fluorophenyl analog (9h) which is the biphenyl analog of potent and efficacious 7ao, was shown to be inactive. Overall, our studies suggest that the aniline NH was not necessary for uncoupling activity.

To advance compounds toward an efficacy study in a mouse model of MASH, we set a threshold of >35% BAM15 OCR activity and <5 μM EC₅₀ and performed pharmacokinetic studies in mice (Table 5). Mice were dosed with single bolus (10 mg kg⁻¹) of 7ao, 7ap, 7al, and 7m. The exposure levels in plasma were determined by liquid chromatography/mass spectrometry (LC/MS) and half-life was calculated. While compounds 7ao, 7ap, and 7al had low exposure levels (4–6 μM), 7m (SHO1122147) had suitable exposure (C_{max} = 35 μM) and half-life of 2.0 h (Figure 4A). With a candidate compound selected, we performed a mitochondrial stress test to determine whether SHO1122147 has protonophore mechanism of action. As expected, the OCR activity of BAM15 was more potent than SHO1122147 (Figure 4B). Blockade of respiration with oligomycin, an ATP synthase inhibitor, at 20 min decreased respiration as judged by the decrease in OCR (Figure 4C). This is expected as protons no longer reenter the mitochondrial matrix via ATP synthase. However, the addition of SHO1122147 or BAM15 (*t* = 40 min) increased OCR suggesting proton transport into the matrix independent of ATP synthase. SHO1122147's OCR activity is lower than the maximum rate for BAM15, and

Table 5. Pharmacokinetic Properties of Select Analogs in Mice

| Compound | Structure | C _{max} (μM) | t _{1/2} (h) |
|--------------------|--------------------------------------------------------------------------------------|-----------------------|----------------------|
| 7ao |  | 6 | 0.9 ± 0.07 |
| 7ap |  | 4 | 1.8 ± 0.25 |
| 7al |  | 4 | 0.9 ± 0.34 |
| (7m) SHO1122147 |  | 35 | 2.0 ± 0.07 |

^aCompounds were administered at 10 mg kg⁻¹ of body weight by oral gavage to C57BL/6 male mice. Plasma samples were collected over 24 h after gavage and analyzed by LC-MS/MS. C_{max} = maximum plasma concentration. t_{1/2} = half-life.

maximum OCR rate is consistent (compare Figure 4B–C). The OCR activity in the presence of oligomycin continued until the addition of complex I and complex III inhibitors (antimycin A and rotenone) where a drop in OCR was observed. These results indicate that the activity of SHO1122147 requires mitochondrial electron transport chain activity. Taken together, our studies indicate that the OCR observed occurs through the mitochondrial electron transport chain with mitochondrial uncoupling activity.

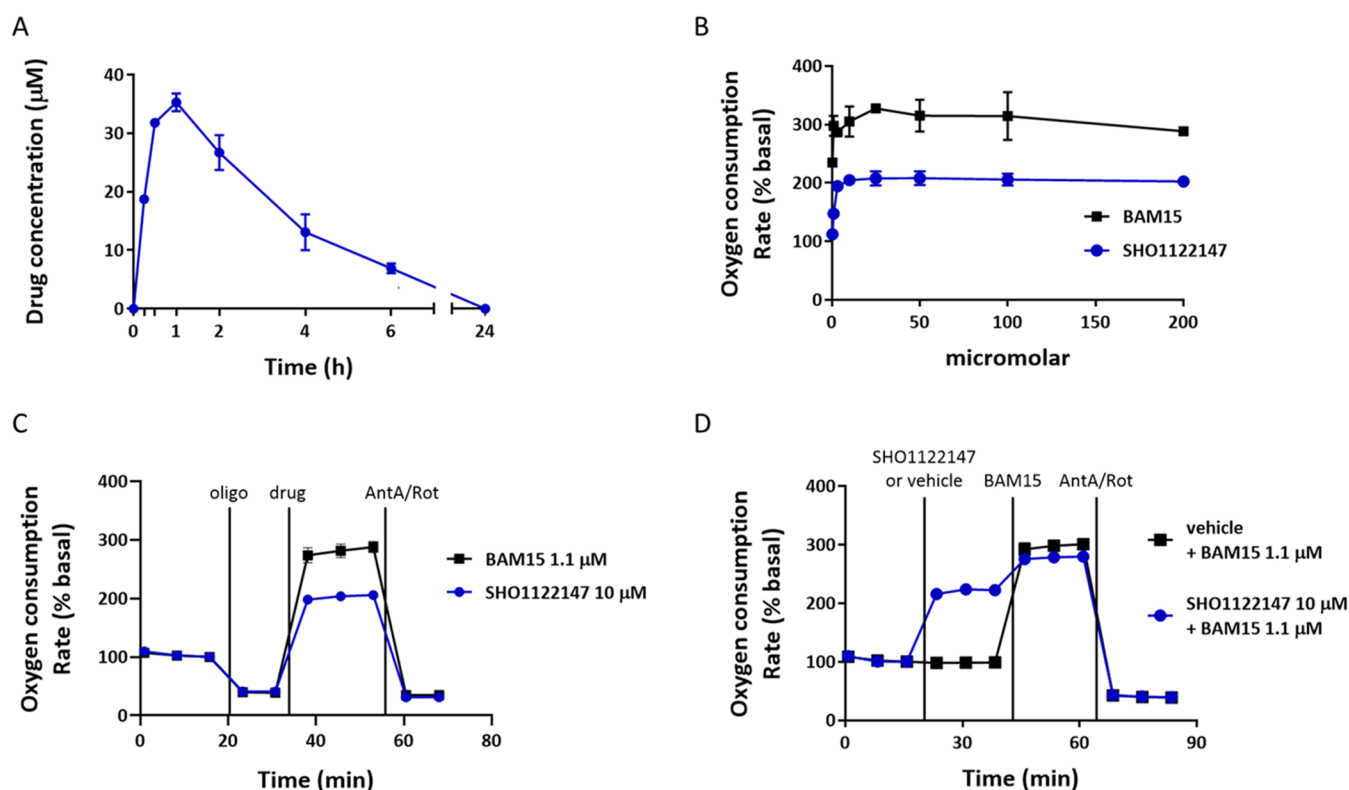


Figure 4. SHO1122147 is an orally bioavailable protonophore. (A) Pharmacokinetic properties of SHO1122147 administered to C57BL/6J male mice by oral gavage at 10 mg kg⁻¹ ($n = 3$). (B) Dose–response curves of SHO1122147 and BAM15-stimulated L6 myoblast cells. (C) Mitochondrial stress test in L6 myoblast cells dosed sequentially with oligomycin (oligo, 1 µM) or vehicle, SHO1122147 (10 µM) or BAM15 (1.1 µM) with vehicle, and antimycin A (AntA, 10 µM) plus rotenone (rot, 1 µM) at the indicated time. $n = 3$ wells per condition. Values are represented as mean \pm standard error of the mean (SEM) (D) Self-limiting test in L6 myoblast cells—dosed with SHO1122147 (10 µM) followed by BAM15 (1.1 µM) and antimycin A (AntA, 10 µM) plus rotenone (Rot, 1 µM) were added at the indicated time. $n = 4$ wells per condition from three separate experiments.

Additionally, SHO1122147 was tested in conjunction with BAM15 to determine whether maximum respiration could be exceeded. As shown in Figure 4D, SHO1122147 alone increases respiration to 200% but upon the addition of BAM15 reaches the maximum of 300%, the same result as when cells are treated with only BAM15. These results suggest that SHO1122147 acts in a self-limiting manner and does not inhibit the maximum mitochondrial respiration.

We next assessed SHO1122147 tolerability in mice by conducting a no observed adverse effect level (NOAEL) study. Rectal temperature, food intake, and body weight were monitored over the course of 24 h after oral dosing with vehicle or SHO1122147 (30, 100, 300, and 1000 mg kg⁻¹) (Figure 5). We observed no changes in temperature, weight, or appetite for all SHO1122147 doses when compared to the vehicle group. These results indicate that the compound was well tolerated acutely at doses up to 1000 mg kg⁻¹.

Finally, we assessed SHO1122147 efficacy in a mouse model of MASH. We utilized the diet induced Gubra-Amylin NASH (GAN) because it is a more clinically relevant model than the chemically induced STAM model used in our past work. Thus, C57BL/6 male mice were fed GAN diet for 33 weeks before the GAN diet was supplemented with or without SHO1122147 at 200 mg kg⁻¹ admixed in food. SHO1122147 was admixed in food due to its 2-h half-life and the 200 mg kg⁻¹ dose was chosen because it was at least 5-fold lower than the maximum tolerated dose. Food intake was monitored daily

during treatment and no significant changes in caloric intake were observed between groups.

Following 4 weeks of compound treatment, we observed that mice fed SHO1122147 had lost 15.4% of body weight (Figure 6A,B). Body composition measured weekly by EchoMRI analysis showed that SHO1122147 treatment improved body composition by lowering fat mass and increasing fat-free lean mass as a percent of body weight (Figure 6C,D). At end of in-life studies, terminal blood was collected and organ weights recorded. Mice treated with SHO1122147 had no significant change in liver mass but showed improvements in fatty liver disease phenotypes including decreased plasma alanine aminotransferase (ALT) and decreased liver triglycerides (Figure 7A–C). Hepatopathological assessment of fixed liver samples revealed a significant decrease of the MAFLD activity score that was primarily due to decreased hepatic steatosis (Figure 7D–G). No changes were observed in the fibrosis stage of SHO1122147 liver samples as compared to GAN controls. These results suggest that mitochondrial uncouplers have the potential to decrease bodyweight and improve MASH score driven by hepatic steatosis.

CONCLUSIONS

There is significant interest in using small molecule mitochondrial uncouplers for the treatment of obesity and accompanying metabolic disorders, such as MASH, due to the novel approach of increasing energy consumption versus

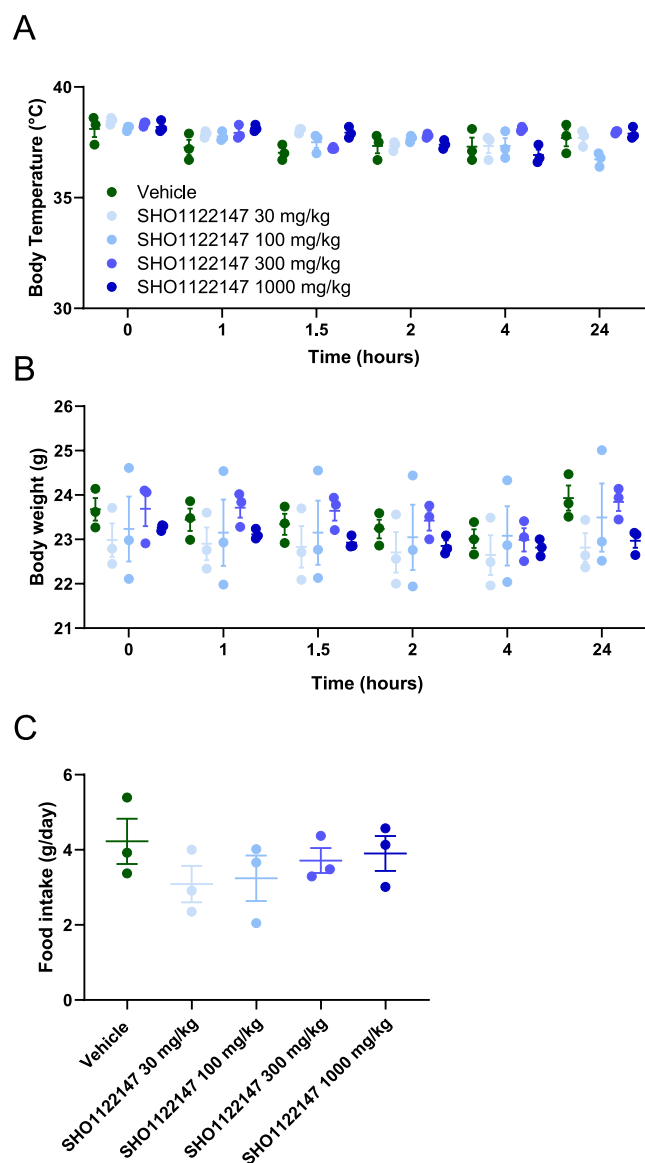


Figure 5. No observed adverse effect level (NOAEL) study with SHO1122147. (A) Body temperature, (B) body weight, and (C) average food intake measurements following administration of vehicle or SHO1122147 at the indicated doses. Values are represented as mean \pm SEM ($n = 3$).

reducing energy intake. Herein, we performed a SAR of a new mitochondrial uncoupler scaffold, [1,2,5]oxadiazolo[3,4-*b*]pyridin-7-ol, where aniline or phenyl derivatives were placed in the 6-position. Our SAR revealed electron withdrawing groups, such as halogens and trifluoromethyl groups on the aniline moiety, afforded mitochondrial uncouplers with moderate EC_{50} values and % BAM15 OCR. In general, the 4-phenylaniline series were better than the aniline and phenyl derivatives, with analogs bearing fluorine or chlorine on the *ortho*- or *para*- positions preferred. Characterization of SHO1122147 confirmed that it is a *bona fide* mitochondrial uncoupler. Efficacy studies in the GAN mouse model demonstrated a decrease in weight, liver fat, and MASH activity score. The ALT and liver triglyceride levels also significantly improved. Overall, these studies suggest the potential of mitochondrial uncouplers as therapeutics for metabolic diseases. Further studies are ongoing to improve the

potency and pharmacokinetic profile of the structure, which will be disclosed in due course.

EXPERIMENTAL SECTION

General Material and Synthetic Procedures. Reagents were obtained from commercial sources unless stated otherwise. Dioxane was deoxygenated by bubbling in argon for 30 min. Toluene was dried using the Innovative Technology Pure SolvMD solvent purification system. Flash silica gel chromatography was performed using SiliaFlash P60 40–63 μm , 60 Å. Thin-layer chromatography was performed to determine the reaction progress utilizing Silicycle aluminum backed silica gel F-254 plates. An Agilent 400-MR 400 MHz or a Varian Inova 400 MHz were used for ^1H and ^{13}C NMR spectroscopic experiments. A Bruker Avance II 500 MHz was predominately utilized for ^{13}C NMR spectroscopic experiments unless stated otherwise. ^1H and ^{13}C NMR spectra are referenced to an internal standard (acetone- d_6), and all chemical shifts are reported in δ ppm. NMR spectra characterizations are presented as follows: chemical shift, multiplicity (s = singlet, d = doublet, t = triplet, q = quartet, dd = doublet of doublets, dt = doublet of triplets, dq = doublet of quartets, tt = triplet of triplets, qd = quartet of doublets, and m = multiplet), coupling constants (Hz), and integration. Purity assessment of compound was performed by Waters UPLC analysis. UPLC conditions: Purity assessments were performed by Waters UPLC analysis. UPLC conditions method one: Solvent A: Water (0.1% TFA); solvent B: acetonitrile (0.1% TFA); column: Acquity BEH C18 1.7 μm 2.1 mm \times 50 mm; method: isocratic 95% A, 5% B from 0 to 3.40 min then linear gradient from 5 to 95% B by 5.10 min, return to 5% B by 5.95 min, then hold for 2 min at 95% A, 5% B; UV wavelength = 280 nm; flow rate: 0.613 mL/min. Method two: Solvent A: Water (0.1% TFA); solvent B: acetonitrile (0.1% TFA); column: Acquity BEH C18 1.7 μm 2.1 mm \times 50 mm; method: isocratic 60% A, 40% B from 0 to 3.50 min then linear gradient from 40 to 95% B by 5 min, return to 40% B by 6 min, then hold for 2 min at 60% A, 40% B; UV wavelength = 280 nm; flow rate: 0.613 mL/min. All final materials synthesized had a purity $\geq 95\%$ as measured by UPLC unless otherwise noted. All compounds tested *in vitro* and *in vivo* are >95 and $>99\%$ pure by HPLC, respectively.

5-Bromo-4-chloro-3-nitropyridin-2-amine (2). To a stirring solution of 4-chloro-3-nitropyridin-2-amine 1 (20.0 g, 115 mmol) in acetonitrile (500 mL) was added *N*-bromosuccinimide (24.6 g, 138 mmol). The reaction was heated under reflux for 1.5 h. The reaction mixture was allowed to cool to 40 $^\circ\text{C}$ and precipitated in cold water (500 mL). The precipitate was filtered, washed twice with water and dried to afford 2 (24.2 g, 95.9 mmol, 83%) as a brown, amorphous solid: ^1H NMR (500 MHz, acetone- d_6) δ 8.43 (s, 1H). ^{13}C NMR (126 MHz, acetone- d_6) δ 153.66, 152.70, 137.97, 107.82. HRMS: (ESI) $[M - \text{H}]^+$ calcd for $\text{C}_5\text{H}_3\text{BrClN}_3\text{O}_2$, 251.9170, observed 251.9170 m/z . Δ 0.0 ppm.

5-Bromo-4-methoxy-3-nitropyridin-2-amine (3). A mixture of 5-bromo-4-chloro-3-nitropyridin-2-amine (2) (47.2 g, 187 mmol) and 25% sodium methoxide in methanol (72.8 g, 337 mmol) in methanol (500 mL) was stirred at 40 $^\circ\text{C}$ for 16 h. The reaction mixture was allowed to cool to room temperature and precipitated in cold water (500 mL). The precipitate was filtered, washed twice with water, and dried to afford 3 (37.2 g, 80%) as a yellow, amorphous solid: ^1H NMR (400 MHz, acetone- d_6) δ 8.29 (s, 1H), 6.74 (s, 2H), 4.03 (s, 3H). ^{13}C NMR (126 MHz, acetone- d_6) δ 159.75, 155.62, 154.29, 127.65, 101.69, 62.84. HRMS: (ESI) $[M + \text{H}]^+$ calcd for $\text{C}_6\text{H}_6\text{BrN}_3\text{O}_3$, 247.9665, observed 247.9664 m/z . Δ -0.4032 ppm.

6-Bromo-7-methoxy-114-[1,2,5]oxadiazolo[4,3-*b*]pyridin-1-olate (4). 5-Bromo-4-methoxy-3-nitropyridin-2-amine 3 (17.0 g, 69.0 mmol) and iodobenzene diacetate (61.8 g, 192 mmol) were added to a round-bottom and stirred in acetonitrile (400 mL) at 80 $^\circ\text{C}$ for 1 h. The reaction was then cooled to room temperature and poured into cold water (500 mL). The acetic acid was quenched with sodium bicarbonate until pH = 7. The reaction mixture was filtered, and the filtrate was extracted with ethyl acetate (4 times). The organic extracts were combined, dried over anhydrous sodium sulfate, concentrated *in*

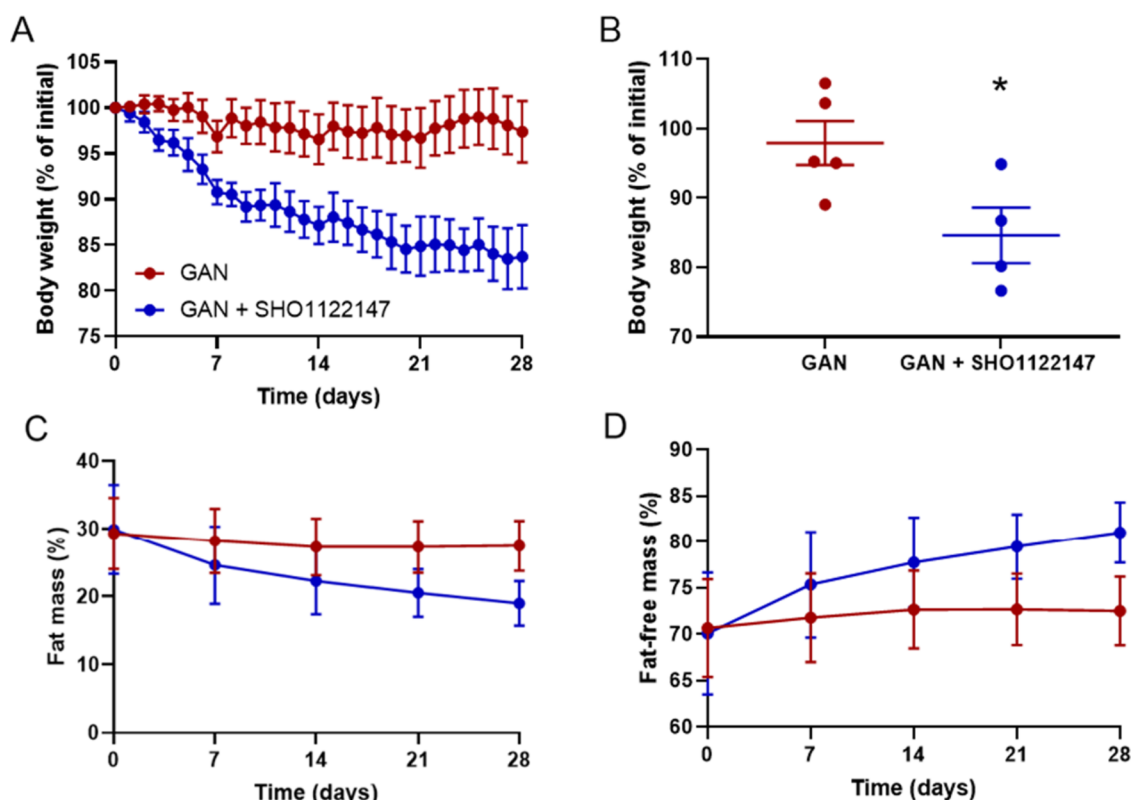


Figure 6. SHO1122147 decreases body weight while improving body composition in the GAN mouse model of NASH. (A, B) Body weight represented as percentage of initial weight (A) over time and (B) at the end of treatment. Measurements of (C) body fat and (D) lean mass represented as percentage of body weight over time. Values are shown as mean \pm SEM ($n = 4-5$). * $p < 0.05$ compared with GAN, determined by unpaired parametric t test (two-tailed).

vacuo, and purified via chromatography on SiO₂ (gradient: 0–15% ethyl acetate/hexanes) to afford **4** (13.1 g, 53 mmol, 77%) as a yellow, amorphous solid: ¹H NMR (500 MHz, acetone-*d*₆) δ 8.58 (s, 1H), 4.69 (s, 3H). ¹³C NMR (126 MHz, acetone-*d*₆) δ 158.88, 154.09, 145.44, 127.69, 106.88, 64.04. HRMS: (ESI) [M + H]⁺ calcd for C₆H₄BrN₃O₃, 245.9509, observed 245.9512 m/z . Δ 1.2197 ppm.

6-Bromo-7-methoxy-[1,2,5]oxadiazolo[3,4-*b*]pyridine (5). To a stirring solution of, 6-bromo-7-methoxy-114-[1,2,5]oxadiazolo[4,3-*b*]pyridin-1-olate **4** (13.0 g, 52.0 mmol) was dissolved in dichloromethane (250 mL) and triphenylphosphine (15.2 g, 58.0 mmol) was added slowly at 0 °C. The mixture was allowed to warm to room temperature and stirred under reflux at 40 °C for 16 h. The reaction was concentrated *in vacuo*, and purified via chromatography on SiO₂ (gradient: 0–10% ethyl acetate/hexanes) to afford **5** (9.1 g, 40 mmol, 75%) as an off-white, amorphous solid: ¹H NMR (400 MHz, acetone-*d*₆) δ 8.91 (s, 1H), 4.69 (s, 4H). ¹³C NMR (101 MHz, acetone-*d*₆) δ 163.61, 161.58, 153.50, 141.40, 105.36, 62.84. HRMS: (ESI) [M + H]⁺ calcd for C₆H₄BrN₃O₂, 229.95597, observed 229.9561 m/z . Δ 0.8697 ppm.

General Procedure for e. To a sealed vial containing Pd₂dba₃ (0.1 equiv), Xantphos (0.2 equiv), 6-bromo-7-methoxy-[1,2,5]oxadiazolo[3,4-*b*]pyridine (**5**) (1.00 equiv), and K₂CO₃ (2.5 equiv) in toluene (0.2 M) was added the aniline derivative (1.1 equiv) under a nitrogen atmosphere with stirring. The reaction mixture was heated under reflux for 14 h. The mixture was allowed to cool to room temperature, concentrated *in vacuo*, and purified via chromatography on SiO₂ (solvent system: ethyl acetate/hexanes) to afford a crude mixture of products **6** and residual aniline.

General Procedure for f. Methoxy derivatives **6** (1 equiv) and Na₂CO₃ (3 equiv) were suspended in dioxane (0.5 mL) and water (0.5 mL). The reaction was heated under reflux for 4 h, then allowed to cool to room temperature, diluted with water, and acidified with 10% aq. HCl. The resulting precipitate was filtered, washed with water, dried, and purified via chromatography on SiO₂ (solvent

system: ethyl acetate/hexanes) to afford the desired products **7**. Yields are listed as combined over two steps.

6-(Phenylamino)-[1,2,5]oxadiazolo[3,4-*b*]pyridin-7-ol (7a). Red solid (19%, 13 mg) ¹H NMR (400 MHz, acetone-*d*₆) δ 8.11 (s, 1H), 8.17 (s, 1H), 7.23–7.14 (m, 2H), 7.06–6.97 (m, 2H), 6.79 (tt, $J = 7.4, 1.1$ Hz, 1H), 6.53 (s, 1H). ¹³C NMR (126 MHz, acetone-*d*₆) δ 168.9, 152.8, 146.4, 145.2, 134.5, 129.9, 126.7, 120.1, 116.7. HRMS: (ESI) [M + H]⁺ calcd for C₁₁H₈N₄O₂, 229.0720, observed 229.0726 m/z . Δ 2.6192 ppm.

6-(*p*-Tolylamino)-[1,2,5]oxadiazolo[3,4-*b*]pyridin-7-ol (7b). Purple solid (8.34%, 10 mg) ¹H NMR (500 MHz, acetone-*d*₆) δ 8.11 (s), 7.03 (d, $J = 8.4$ Hz, 2H), 6.96 (d, $J = 8.4$ Hz, 2H), 6.43 (s), 2.23 (s). ¹³C NMR (500 MHz, acetone-*d*₆) δ 151.9, 144.0, 142.5, 131.6, 129.5, 128.9, 126.9, 116.5, 116.4, 19.68. HRMS: ESI [M + H]⁺ calc for C₁₂H₁₀N₄O₂, 243.0877, observed, 243.0879. m/z . Δ 0.8227 ppm.

6-((4-Ethylphenyl)amino)-[1,2,5]oxadiazolo[3,4-*b*]pyridin-7-ol (7c). Red solid (18%, 31 mg) ¹H NMR (500 MHz, acetone-*d*₆) δ 11.14 (s, 1H), 8.12 (s, 1H), 7.07 (d, $J = 8.5$ Hz, 2H), 6.99 (d, $J = 8.5$ Hz, 2H), 6.44 (s, 2H), 2.54 (q, $J = 7.6$ Hz, 2H), 1.17 (t, $J = 7.6$ Hz, 3H). ¹³C NMR (126 MHz, acetone-*d*₆) δ 151.8, 144.0, 142.7, 135.7, 128.4, 126.9, 119.7, 116.5, 27.8, 15.5. HRMS: (ESI) [M + H]⁺ calcd for C₁₃H₁₂N₄O₂, 255.08875, observed 255.0891 m/z . Δ 1.3720 ppm.

6-((4-Butylphenyl)amino)-[1,2,5]oxadiazolo[3,4-*b*]pyridin-7-ol (7d). Purple solid (33%, 47 mg) ¹H NMR (600 MHz, acetone-*d*₆) δ 11.14 (s, 1H), 8.12 (s, 4H), 7.05 (d, $J = 8.7$ Hz, 9H), 6.98 (d, $J = 2.3$ Hz, 9H), 6.43 (s, 3H), 2.52 (t, $J = 7.7$ Hz, 9H), 1.61–1.49 (m, 10H), 1.34 (h, $J = 15.1$ Hz, 10H), 0.91 (t, $J = 7.8$ Hz, 14H). ¹³C NMR (126 MHz, acetone-*d*₆) δ 168.5, 152.6, 145.0, 143.6, 135.1, 132.0, 129.9, 127.9, 117.3, 35.4, 34.8, 22.9, 14.2. HRMS: ESI [M + H]⁺ calc for C₁₅H₁₃N₅O₂, 285.1346, observed, 285.1355. m/z . Δ 3.1564 ppm.

6-((4-*tert*-Butylphenyl)amino)-[1,2,5]oxadiazolo[3,4-*b*]pyridin-7-ol (7e). Purple solid (29%, 28 mg) ¹H NMR (600 MHz, acetone-*d*₆) δ 8.14 (s, 1H), 7.25 (d, $J = 2.9, 2.2$ Hz, 2H), 6.98 (dd, $J = 2.9, 2.2$ Hz, 2H), 6.45 (s, 1H), 1.27 (s, 9H). ¹³C NMR (126 MHz, acetone-

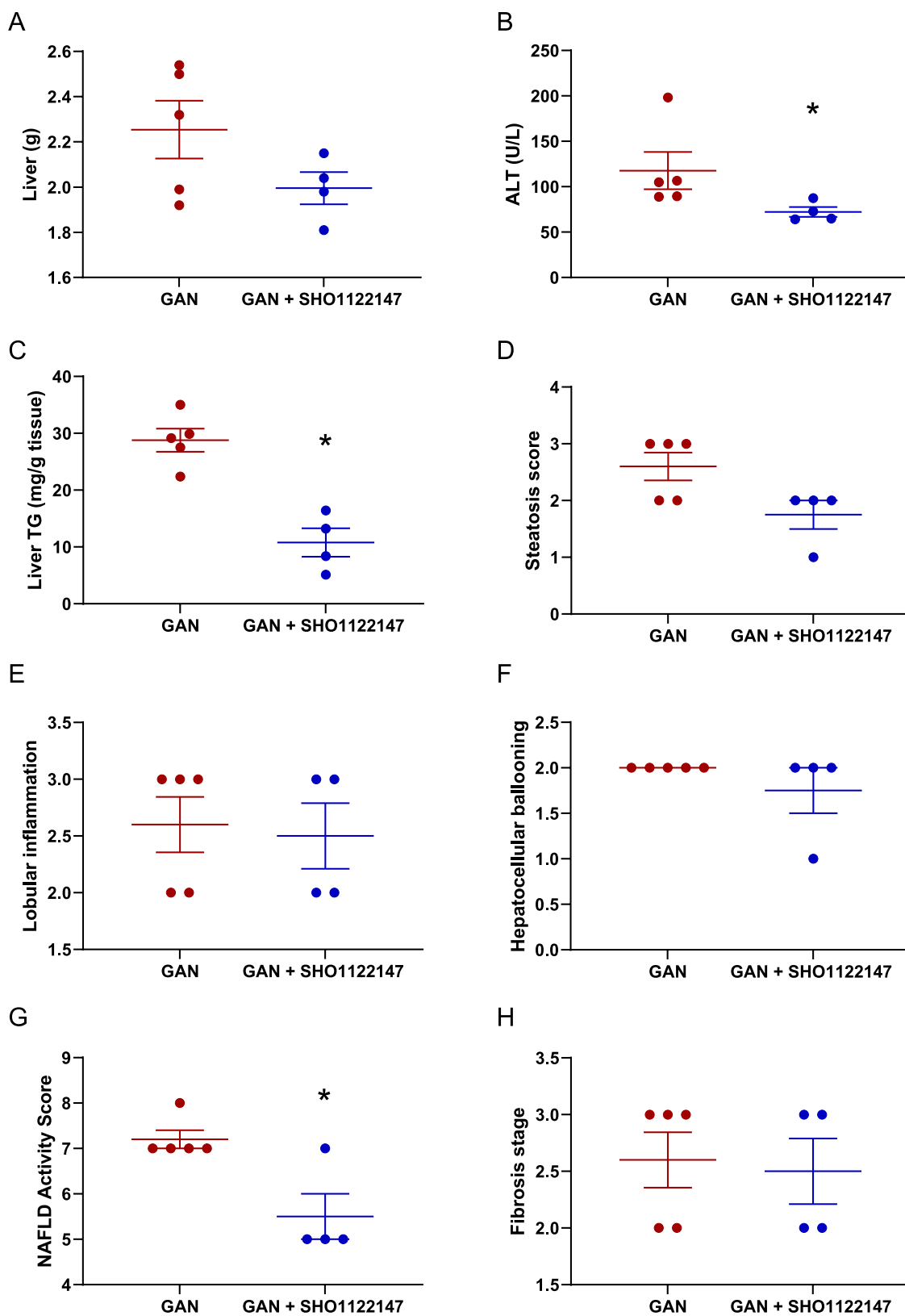


Figure 7. SHO1122147 decreases liver steatosis and lowers ALT in a mouse model of NASH. (A) Liver weight and (B) plasma alanine aminotransferase (ALT) activity levels. (C) Liver triglycerides (TG) at the end of the study. (D–F) Individual and (G) composite NAFLD activity scores. (H) Liver fibrosis stage. Values are represented as mean \pm SEM ($n = 4–5$). * $p < 0.05$ compared with GAN, determined by (C) unpaired parametric t test (two-tailed) and (B, G) Mann–Whitney nonparametric test.

*d*₆) δ 168.2, 152.7, 144.9, 143.3, 143.3, 132.7, 127.7, 126.7, 119.9, 116.9, 34.5, 31.8. HRMS: ESI $[M + H]^+$ calc for C₁₅H₁₆N₄O₂, 285.1346, observed, 285.1353 *m/z*. Δ 2.4550 ppm.

6-((4-Butoxyphenyl)amino)-[1,2,5]oxadiazolo[3,4-*b*]pyridin-7-ol (7f). Purple solid (61%, 96 mg) ¹H NMR (600 MHz, acetone-*d*₆) δ 11.05 (s, 1H), 7.09 (d, *J* = 9.0, 5.8, 3.6 Hz, 2H), 6.87 (d, *J* = 8.9, 5.8, 3.6 Hz, 2H), 6.33 (s, 1H), 3.96 (t, *J* = 6.4 Hz, 2H), 1.74 (m, 2H), 1.50 (h, *J* = 15.0, 7.5 Hz, 2H), 0.99 (t, *J* = 7.4 Hz, 3H). ¹³C NMR (126 MHz, acetone-*d*₆) δ 154.1, 151.6, 143.7, 137.3, 128.8, 127.9, 120.0, 119.6, 115.2, 67.6, 31.3, 19.0, 13.2. HRMS: ESI $[M + H]^+$ calc for C₁₅H₁₆N₄O₃, 301.1295, observed, 301.1298. *m/z*. Δ 0.9962 ppm.

2-((4-(7-Hydroxy-[1,2,5]oxadiazolo[3,4-*b*]pyridin-6-yl)amino)phenyl)-2-methylpropanenitrile (7g). Purple solid (82%, 43 mg) ¹H NMR (600 MHz, acetone-*d*₆) δ 8.19 (s), 7.31 (d, *J* = 8.5, 5.1, 3.0 Hz, 2H), 6.99 (d, *J* = 8.5, 5.1, 3.0 Hz, 2H), 6.68 (s), 1.66 (s, 6H). ¹³C NMR (600 MHz, acetone-*d*₆) δ 168.12, 152.1, 145.5, 144.6, 135.7, 132.2, 125.9, 125.1, 124.7, 115.2, 36.2, 28.4. HRMS: ESI $[M + H]^+$ calc for C₁₅H₁₃N₅O₂, 296.1142, observed, 296.1147. *m/z*. Δ 1.6885 ppm.

6-((4-(Trifluoromethyl)thio)phenyl)amino)-[1,2,5]oxadiazolo[3,4-*b*]pyridin-7-ol (7h). Red solid (65%, 187 mg) ¹H NMR (400 MHz, acetone-*d*₆) δ 11.50 (s, 1H), 8.29 (d, *J* = 2.2 Hz, 1H), 7.43 (dd, *J* = 4.8, 2.4 Hz, 2H), 7.11 (s, 1H), 6.98 (d, *J* = 10.1 Hz, 2H). ¹⁹F NMR (376 MHz, acetone) δ -45.5. ¹³C NMR (126 MHz, acetone-*d*₆) δ 169.6, 153.3, 150.9, 146.0, 140.5, 138.8, 130.9 (q, *J* = 307.1 Hz), 124.1, 115.7, 110.8. HRMS: (ESI) $[M + H]^+$ calc for C₁₂H₇F₃N₄O₂S 329.0314 observed 329.0317 *m/z*. Δ 0.9117 ppm.

4-((7-Hydroxy-[1,2,5]oxadiazolo[3,4-*b*]pyridin-6-yl)amino)benzonitrile (7i). Red solid (23%, 52 mg) ¹H NMR (500 MHz, acetone-*d*₆) δ 11.56 (s, 1H), 8.29 (s, 1H), 7.47 (d, *J* = 8.7 Hz, 2H), 7.31 (s, 1H), 6.96 (d, *J* = 8.8 Hz, 2H). ¹³C NMR (126 MHz, acetone-*d*₆) δ 153.4, 152.0, 146.1, 141.3, 134.1, 123.4, 120.5, 114.9, 100.8. HRMS: (ESI) $[M - H]^-$ calc for C₁₂H₇N₅O₂ 252.0527 observed 252.0517 *m/z*. Δ -3.9674 ppm.

1-((4-(7-Hydroxy-[1,2,5]oxadiazolo[3,4-*b*]pyridin-6-yl)amino)phenyl)ethan-1-one (7j). Yellow solid (62%, 88 mg) ¹H NMR (400 MHz, acetone-*d*₆) δ 8.16 (s, 1H), 7.83 (d, *J* = 8.8 Hz, 2H), 6.77 (d, *J* = 8.7 Hz, 2H), 2.49 (s, 3H). ¹³C NMR (126 MHz, MeOD) δ 153.4, 131.9, 128.4, 123.5, 114.0, 26.1. HRMS: (ESI) $[M - H]^-$ calc for C₁₃H₁₀N₄O₃, 269.0680, observed 269.0677 *m/z*. Δ -1.1149 ppm
*Not all carbon peaks observed.

6-((6-Fluoropyridin-3-yl)amino)-[1,2,5]oxadiazolo[3,4-*b*]pyridin-7-ol (7k). Red solid (31%, 60 mg) ¹H NMR (500 MHz, acetone-*d*₆) δ 11.38 (s, 1H), 8.22 (s, 1H), 7.85 (t, *J* = 2.6 Hz, 1H), 7.50 (ddd, *J* = 8.7, 6.9, 3.1 Hz, 1H), 6.87 (dd, *J* = 8.8, 3.4 Hz, 1H), 6.76 (s, 1H), (d, *J* = 4.0 Hz), 137.3, 134.6 (d, *J* = 15.7 Hz), 128.8 (d, *J* = 7.3 Hz), 125.8, 109.7 (d, *J* = 40.3 Hz). ¹⁹F NMR (376 MHz, Acetone-*d*₆) δ -58.8. ¹³C NMR (126 MHz, acetone-*d*₆) δ 169.3, 158.3 (d, *J* = 227.2 Hz), 153.1, 145.7, 141.9. HRMS: (ESI) $[M - H]^-$ calc for C₁₀H₆FN₅O₂, 248.0579, observed 248.0578 *m/z*. Δ -0.4031 ppm.

6-((6-(Trifluoromethyl)pyridin-3-yl)-[1,2,5]oxadiazolo[3,4-*b*]pyridin-7-ol (7l). Yellow solid (36%, 67 mg) ¹H NMR (500 MHz, acetone-*d*₆) δ 11.94 (s, 1H), 8.98 (d, *J* = 2.2 Hz, 1H), 8.55 (s, 1H), 8.35 (ddd, *J* = 8.2, 2.2, 0.8 Hz, 1H), 7.91 (dd, *J* = 8.2, 0.8 Hz, 1H). ¹⁹F NMR (376 MHz, acetone) δ -68.30. ¹³C NMR (126 MHz, acetone-*d*₆) δ 170.9, 153.7, 150.4, 146.8 (d, *J* = 34.5 Hz), 146.0, 144.3, 138.5, 134.4, 122.9 (d, *J* = 273.2 Hz), 120.8 (d, *J* = 2.9 Hz), 118.9. HRMS: (ESI) $[M - H]^-$ calc for C₁₁H₅F₃N₄O₂, 283.0437, observed 283.0437 *m/z*. Δ 0.0 ppm.

6-((2-Fluorophenyl)amino)-[1,2,5]oxadiazolo[3,4-*b*]pyridin-7-ol (7m). Purple solid (21%, 35 mg) ¹H NMR (400 MHz, acetone-*d*₆) δ 11.34 (s, 1H), 8.18 (d, *J* = 1.3 Hz, 1H), 7.14–6.99 (m, 2H), 6.85–6.75 (m, 1H), 6.28 (s, 1H). ¹⁹F NMR (376 MHz, acetone-*d*₆) δ -134.3. ¹³C NMR (126 MHz, acetone-*d*₆) δ 153.7 (d, *J* = 148.2 Hz), 152.4, 145.5, 136.8, 134.9, 125.5, 125.4 (d, *J* = 3.5 Hz), 120.4 (d, *J* = 6.9 Hz), 116.9 (d, *J* = 2.8 Hz), 115.8 (d, *J* = 19.6 Hz). HRMS: (ESI) $[M - H]^-$ calc for C₁₁H₇FN₄O₂, 245.0480, observed 245.0480 *m/z*. Δ 0.0 ppm.

6-((3-Fluorophenyl)amino)-[1,2,5]oxadiazolo[3,4-*b*]pyridin-7-ol (7n). Red solid (23%, 36 mg) ¹H NMR (400 MHz, acetone-*d*₆) δ 11.34 (s, 1H), 8.23 (d, *J* = 0.6 Hz, 1H), 7.15 (td, *J* = 8.2, 6.8 Hz, 1H),

6.77 (ddd, *J* = 8.2, 2.2, 0.9 Hz, 2H), 6.68 (dt, *J* = 11.9, 2.3 Hz, 1H), 6.46 (dddd, *J* = 8.9, 8.1, 2.5, 0.9 Hz, 1H). ¹⁹F NMR (376 MHz, acetone-*d*₆) δ -114.6. ¹³C NMR (126 MHz, acetone-*d*₆) δ 169.49, 164.8 (d, *J* = 240.9 Hz), 153.2, 149.7 (d, *J* = 8.9 Hz), 145.8, 138.3, 131.2 (d, *J* = 10.0 Hz), 125.3, 111.6, 105.7 (d, *J* = 21.5 Hz), 102.0 (d, *J* = 25.4 Hz). HRMS: (ESI) $[M - H]^-$ calc for C₁₁H₇FN₄O₂, 245.0480 observed 245.0471 *m/z*. Δ -3.6727 ppm.

6-((4-Fluorophenyl)amino)-[1,2,5]oxadiazolo[3,4-*b*]pyridin-7-ol (7o). Purple solid (11%, 11 mg) ¹H NMR (500 MHz, acetone-*d*₆) δ 11.26 (s, 1H), 8.14 (s, 1H), 7.09–6.89 (m, 4H), 6.56 (s, 1H). ¹⁹F NMR (376 MHz, acetone-*d*₆) δ -126.6 (tt, *J* = 8.8, 4.7 Hz). ¹³C NMR (126 MHz, acetone-*d*₆) δ 168.7, 157.67 (d, *J* = 235.4 Hz), 152.9, 145.3, 142.9, 134.6, 127.2, 118.1 (d, *J* = 7.6 Hz), 116.2 (d, *J* = 22.5 Hz). HRMS: (ESI) $[M - H]^-$ calc for C₁₁H₇FN₄O₂, 247.0625, observed 247.0626 *m/z*. Δ 0.4047 ppm.

6-((2-Chlorophenyl)amino)-[1,2,5]oxadiazolo[3,4-*b*]pyridin-7-ol (7p). Yellow solid (62%, 56 mg) ¹H NMR (400 MHz, acetone-*d*₆) δ 11.37 (s, 1H), 8.26 (d, *J* = 0.7 Hz, 1H), 7.34 (dd, *J* = 7.9, 1.6 Hz, 1H), 7.11 (dddd, *J* = 7.9, 7.3, 1.5, 0.5 Hz, 1H), 6.96 (dd, *J* = 8.2, 1.6 Hz, 1H), 6.78 (ddd, *J* = 7.9, 7.3, 1.5 Hz, 1H). ¹³C NMR (126 MHz, acetone-*d*₆) δ 153.4, 145.8, 143.3, 139.1, 130.3, 128.7, 124.8, 121.0, 120.5, 115.4. HRMS: (ESI) $[M + H]^+$ calc for C₁₁H₇ClN₄O₂ 263.0330 observed 263.0340 *m/z*. Δ 3.6877 ppm.

6-((2-(Trifluoromethyl)phenyl)amino)-[1,2,5]oxadiazolo[3,4-*b*]pyridin-7-ol (7q). Purple solid (35%, 44 mg) ¹H NMR (400 MHz, acetone-*d*₆) δ 11.47 (s, 1H), 8.26 (s, 1H), 7.56 (dd, *J* = 8.0, 1.6 Hz, 1H), 7.38 (t, *J* = 7.4 Hz, 1H), 7.10 (s, 1H), 6.92 (ddt, *J* = 8.1, 7.2, 1.0 Hz, 1H), 6.42 (s, 1H). ¹⁹F NMR (376 MHz, acetone-*d*₆) δ -62.4. ¹³C NMR (126 MHz, acetone-*d*₆) δ 169.1, 153.3, 145.7, 145.1, 139.3, 134.0, 127.3 (q, *J* = 5.4 Hz), 126.1 (d, *J* = 271.6 Hz), 124.5, 119.5, 116.6, 116.0 (d, *J* = 29.4 Hz). HRMS: (ESI) $[M - H]^-$ calc for C₁₂H₇F₃N₄O₂, 295.0448, observed 295.0442 *m/z*. Δ -2.0335 ppm.

6-((3-(Trifluoromethyl)phenyl)amino)-[1,2,5]oxadiazolo[3,4-*b*]pyridin-7-ol (7r). Red solid (56%) ¹H NMR (400 MHz, acetone-*d*₆) δ 11.37 (s, 1H), 8.28 (d, *J* = 0.7 Hz, 1H), 7.34 (t, *J* = 8.1, 7.6 Hz, 1H), 7.23–7.10 (m, 2H), 7.08–6.99 (m, 1H), 6.93 (s, 1H). ¹⁹F NMR (376 MHz, acetone-*d*₆) δ -63.3. ¹³C NMR (126 MHz, acetone-*d*₆) δ 153.3, 148.5, 145.9, 139.4, 131.7 (d, *J* = 31.5 Hz), 130.6, 125.5 (d, *J* = 271.9 Hz), 124.8 (d, *J* = 265.2 Hz), 118.7, 115.5 (q, *J* = 4.3 Hz), 111.5 (q, *J* = 4.3 Hz). HRMS: (ESI) $[M - H]^-$ calc for C₁₂H₇F₃N₄O₂, 295.0448, observed 295.0440 *m/z*. Δ -2.7114 ppm.

6-((4-(Trifluoromethyl)phenyl)amino)-[1,2,5]oxadiazolo[3,4-*b*]pyridin-7-ol (7s). Red solid (84%, 78 mg) ¹H NMR (500 MHz, acetone-*d*₆) δ 11.45 (s, 1H), 8.29 (s, 1H), 7.43 (d, *J* = 8.4 Hz, 2H), 7.09 (s, 1H), 7.01 (d, *J* = 8.4 Hz, 2H). ¹⁹F NMR (376 MHz, acetone-*d*₆) δ -61.5. ¹³C NMR (126 MHz, acetone-*d*₆) δ 169.56, 153.34, 151.18, 146.00, 140.18, 127.09 (d, *J* = 4.1 Hz), 125.74 (d, *J* = 271.4 Hz), 124.29, 120.05 (d, *J* = 32.4 Hz), 114.63. HRMS: (ESI) $[M - H]^-$ calc for C₁₂H₇F₃N₄O₂, 295.0443, observed 295.0450 *m/z*. Δ 2.4 ppm.

6-((2,3-Difluorophenyl)amino)-[1,2,5]oxadiazolo[3,4-*b*]pyridin-7-ol (7t). Purple solid (38%, 66 mg) ¹H NMR (400 MHz, acetone-*d*₆) δ 11.43 (s, 1H), 8.24 (d, *J* = 0.8 Hz, 1H), 6.92 (dddd, *J* = 11.0, 8.6, 5.7, 2.3 Hz, 1H), 6.78–6.56 (m, 3H). ¹⁹F NMR (376 MHz, acetone-*d*₆) δ -141.8, -161.1. ¹³C NMR (126 MHz, acetone-*d*₆) δ 169.8, 153.8, 152.3 (dd, *J* = 242.8, 10.5 Hz), 146.4, 141.6 (dd, *J* = 240.2, 15.3 Hz), 140.2, 138.2 (d, *J* = 8.1 Hz), 125.3 (dd, *J* = 8.8, 4.8 Hz), 124.9, 112.2, 107.6 (d, *J* = 17.5 Hz). HRMS: (ESI) $[M - H]^-$ calc for C₁₁H₆F₂N₄O₂ 263.0386 observed 263.0387 *m/z*. Δ 0.3801 ppm.

6-((2,4-Difluorophenyl)amino)-[1,2,5]oxadiazolo[3,4-*b*]pyridin-7-ol (7u). Purple solid (17%, 29 mg) ¹H NMR (500 MHz, acetone-*d*₆) δ 11.31 (s, 1H), 8.11 (s, 1H), 7.1–7.04 (m, 2H), 6.87–6.76 (m, 1H), 6.36–6.28 (m, 1H). ¹⁹F NMR (376 MHz, acetone-*d*₆) δ -123.7 (dd, *J* = 8.8, 6.1 Hz), -128.6 (t, *J* = 10.9 Hz). ¹³C NMR (126 MHz, acetone) δ 157.1 (dd, *J* = 238.8, 11.0 Hz), 153.3 (dd, *J* = 243.7, 12.0 Hz), 153.2, 145.54, 136.2, 132.5–130.0 (m), 126.2, 118.6 (dd, *J* = 9.0, 4.0 Hz), 111.7 (dd, *J* = 21.8, 3.7 Hz), 104.63 (dd, *J* = 26.9, 23.3 Hz). HRMS: (ESI) $[M - H]^-$ calc for C₁₁H₆F₂N₄O₂ 263.0386 observed 263.0388 *m/z*. Δ 0.7603 ppm.

6-((2,5-Difluorophenyl)amino)-[1,2,5]oxadiazolo[3,4-*b*]pyridin-7-ol (7v). Purple solid (43%, 74 mg) ¹H NMR (400 MHz, acetone-

δ 11.44 (s, 1H), 8.27 (d, $J = 0.8$ Hz, 1H), 7.06 (ddd, $J = 11.3, 8.9, 5.1$ Hz, 1H), 6.66 (ddd, $J = 10.4, 7.1, 3.1$ Hz, 1H), 6.43 (ddt, $J = 8.9, 8.1, 3.3$ Hz, 1H). ^{19}F NMR (376 MHz, acetone- d_6) δ -119.4 to -119.6 (m), -141.2. ^{13}C NMR (126 MHz, acetone- d_6) δ 169.5, 160.4 (d, $J = 243.6$ Hz), 153.4, 148.6 (d, $J = 243.6$ Hz), 146.1, 140.6, 138.2–135.8 (m), 123.8, 116.2 (dd, $J = 21.3, 10.5$ Hz), 104.5 (dd, $J = 24.8, 7.4$ Hz), 102.7 (dd, $J = 29.0, 3.4$ Hz). HRMS: (ESI) $[\text{M} - \text{H}]^-$ calcd for $\text{C}_{11}\text{H}_6\text{F}_2\text{N}_4\text{O}_2$, 263.03861, observed 263.0377 m/z . Δ -3.4595 ppm.

6-((2,6-Difluorophenyl)amino)-[1,2,5]oxadiazolo[3,4-*b*]pyridin-7-ol (7w). Red solid (22% yield, 23 mg) ^1H NMR (500 MHz, acetone- d_6) δ 11.20 (s, 1H), 7.69 (s, 1H), 7.14–6.99 (m, 3H), 6.37 (s, 1H). ^{13}C NMR (126 MHz, acetone- d_6) δ 167.37, 156.77 (dd, $J = 244.8, 6.2$ Hz), 152.56, 144.51, 129.07, 128.54, 123.59 (t, $J = 9.7$ Hz), 121.34 (t, $J = 15.0$ Hz), 112.77 (dd, $J = 18.1, 5.5$ Hz). HRMS: (ESI) $[\text{M} - \text{H}]^+$ calcd for $\text{C}_{11}\text{H}_6\text{F}_2\text{N}_4\text{O}_2$ 265.0532 observed 265.0533 m/z . Δ 0.3772 ppm.

6-((3,4-Difluorophenyl)amino)-[1,2,5]oxadiazolo[3,4-*b*]pyridin-7-ol (7x). Purple solid (57%, 98 mg) ^1H NMR (400 MHz, acetone- d_6) δ 11.36 (s, 1H), 8.22 (d, $J = 0.6$ Hz, 1H), 7.09 (dt, $J = 10.6, 9.0$ Hz, 1H), 6.86 (ddd, $J = 13.2, 6.9, 2.8$ Hz, 1H), 6.76–6.69 (m, 2H). ^{19}F NMR (376 MHz, acetone- d_6) δ -139.6, -153.4. ^{13}C NMR (126 MHz, acetone- d_6) δ 169.4, 153.2, 151.3 (dd, $J = 242.8, 13.5$ Hz), 145.8, 144.9 (d, $J = 8.4$ Hz), 144.3 (dd, $J = 235.9, 12.9$ Hz), 138.2, 125.6, 118.1 (d, $J = 18.0$ Hz), 111.5 (d, $J = 2.6$ Hz), 104.2 (d, $J = 20.9$ Hz). HRMS: (ESI) $[\text{M} - \text{H}]^-$ calcd for $\text{C}_{11}\text{H}_6\text{F}_2\text{N}_4\text{O}_2$ 263.0386 observed 263.0387 m/z . Δ 0.3801 ppm.

6-((2,3,4-Trifluorophenyl)amino)-[1,2,5]oxadiazolo[3,4-*b*]pyridin-7-ol (7y). Purple solid (22%, 26 mg) ^1H NMR (400 MHz, acetone- d_6) δ 8.20 (s, 1H), 6.94 (ddd, $J = 10.3, 9.4, 8.1, 2.4$ Hz, 1H), 6.73 (tdd, $J = 9.3, 4.9, 2.5$ Hz, 1H), 6.56 (s, 1H). ^{19}F NMR (376 MHz, acetone- d_6) δ -148.7 to -152.1 (m), -153.3 to -157.4 (m), -163.7 (td, $J = 20.7, 19.9, 7.7$ Hz). ^{13}C NMR (126 MHz, acetone- d_6) δ 169.2, 153.3, 145.8, 145.0 (dd, $J = 238.7, 9.3$ Hz), 142.1 (dd, $J = 244.4, 12.8$ Hz), 140.9 (dd, $J = 245.5, 5.2$ Hz), 139.2, 133.5 (d, $J = 8.7$ Hz), 124.6, 112.1 (dd, $J = 17.7, 3.8$ Hz), 110.6 (dt, $J = 6.8, 3.3$ Hz). HRMS: (ESI) $[\text{M} + \text{H}]^+$ calcd for $\text{C}_{11}\text{H}_5\text{F}_3\text{N}_4\text{O}_2$ 283.0437 observed 283.0441 m/z . Δ 1.4132 ppm.

6-((Perfluorophenyl)amino)-[1,2,5]oxadiazolo[3,4-*b*]pyridin-7-ol (7z). Orange solid (58%, 91 mg) ^1H NMR (500 MHz, DMSO) δ 12.75 (s, 1H), 8.07 (s, 1H), 7.68 (s, 1H). ^{19}F NMR (376 MHz, acetone) δ -155.6 (d, $J = 22.3$ Hz), -166.7 (td, $J = 20.8, 4.1$ Hz), -170.4 (tt, $J = 21.4, 4.4$ Hz). ^{13}C NMR (126 MHz, DMSO) δ 167.1, 151.9, 144.3, 138.8 (d, $J = 241.2$ Hz), 138.4, 136.4, 133.6 (d, $J = 241.4$ Hz), 124.5, 121.3. HRMS: (ESI) $[\text{M} - \text{H}]^-$ calcd for $\text{C}_{11}\text{H}_3\text{F}_5\text{N}_4\text{O}_2$, 317.01034, observed 317.0095 m/z . Δ -2.6497 ppm.

6-((3-Chloro-2-fluorophenyl)amino)-[1,2,5]oxadiazolo[3,4-*b*]pyridin-7-ol (7aa). Red solid (58%, 116 mg) ^1H NMR (400 MHz, Acetone- d_6) δ 11.43 (s, 1H), 8.25 (d, $J = 0.8$ Hz, 1H), 6.97–6.78 (m, 3H), 6.62 (s, 1H). ^{19}F NMR (376 MHz, acetone- d_6) δ -137.6. ^{13}C NMR (126 MHz, acetone- d_6) δ 169.3, 153.3, 148.4 (d, $J = 241.4$ Hz), 145.9, 140.1, 137.2 (d, $J = 10.6$ Hz), 125.6 (d, $J = 4.7$ Hz), 124.2, 121.0 (d, $J = 15.1$ Hz), 120.0, 114.9. HRMS: (ESI) $[\text{M} + \text{H}]^+$ calcd for 281.0236 observed 281.0241 m/z . Δ 1.7436 ppm.

6-((2-Fluoro-3-(trifluoromethyl)phenyl)amino)-[1,2,5]oxadiazolo[3,4-*b*]pyridin-7-ol (7ab). Red solid (55%, 112 mg) ^1H NMR (500 MHz, acetone- d_6) δ 11.50 (s, 1H), 8.30 (d, $J = 0.8$ Hz, 1H), 7.24–7.08 (m, 2H), 7.02 (td, $J = 7.3, 1.3$ Hz, 1H), 6.80 (s, 1H). ^{19}F NMR (376 MHz, acetone- d_6) δ -61.6 (d, $J = 13.0$ Hz), -137.1 to -140.8 (m). ^{13}C NMR (126 MHz, acetone- d_6) δ 169.5, 153.5, 149.4 (d, $J = 248.0$ Hz), 146.1, 141.2, 137.2 (d, $J = 9.9$ Hz), 125.3 (d, $J = 4.4$ Hz), 124.1 (q, $J = 271.4$ Hz), 123.6, 120.1 (d, $J = 4.0$ Hz), 118.3 (qd, $J = 33.2, 32.6, 10.2$ Hz), 115.7 (q, $J = 4.7$ Hz). HRMS: (ESI) $[\text{M} - \text{H}]^-$ calcd for $\text{C}_{12}\text{H}_6\text{F}_4\text{N}_4\text{O}_2$ 313.03541 observed 313.0348 m/z . Δ -1.9486 ppm.

6-((2-Fluoro-5-(trifluoromethyl)phenyl)amino)-[1,2,5]oxadiazolo[3,4-*b*]pyridin-7-ol (7ac). Purple solid (43%, 67 mg) ^1H NMR (400 MHz, acetone- d_6) δ 11.48 (s, 1H), 8.34 (d, $J = 0.7$ Hz, 1H), 7.26 (dddd, 1H), 7.15 (dd, $J = 8.1, 1.4$ Hz, 1H), 7.12–7.0 (m, 1H), 6.78–6.60 (m, 1H). ^{19}F NMR (376 MHz, acetone- d_6) δ -62.5,

-130.1 (d, $J = 12.0$ Hz) ^{13}C NMR (126 MHz, acetone- d_6) δ 169.7, 154.3 (d, $J = 245.3$ Hz), 153.4, 146.1, 141.6, 136.9 (d, $J = 11.9$ Hz), 127.3 (qd, $J = 32.2, 3.4$ Hz), 125.1 (q, $J = 271.3$ Hz), 123.3, 116.3, 116.1, 112.5 (t, $J = 4.0$ Hz). HRMS: (ESI) $[\text{M} - \text{H}]^-$ calcd for $\text{C}_{12}\text{H}_6\text{F}_4\text{N}_4\text{O}_2$, 313.0354, observed 313.0350 m/z . Δ -1.2778 ppm.

6-((2-Fluoro-6-(trifluoromethyl)phenyl)amino)-[1,2,5]oxadiazolo[3,4-*b*]pyridin-7-ol (7ad). Orange solid (32%, 34 mg) ^1H NMR (500 MHz, DMSO) δ 12.51 (s, 1H), 7.70 (s, 1H), 7.53–7.43 (m, 2H), 7.28–7.14 (m, 1H), 6.86 (s, 1H). ^{19}F NMR (376 MHz, DMSO) δ -58.9, -116.3 (d, $J = 11.3$ Hz). ^{13}C NMR (126 MHz, DMSO) δ 165.8, 156.2 (d, $J = 246.6$ Hz), 151.5, 143.9, 131.1, 130.2 (d, $J = 12.6$ Hz), 127.8, 123.9 (q, $J = 272.8$ Hz), 123.5, 122.6, 120.7 (d, $J = 20.4$ Hz). HRMS: (ESI) $[\text{M} - \text{H}]^-$ calcd for $\text{C}_{12}\text{H}_6\text{F}_4\text{N}_4\text{O}_2$, 313.0354, observed 313.0345 m/z . Δ -2.8750 ppm.

6-((2,4-Difluoro-5-(trifluoromethyl)phenyl)amino)-[1,2,5]oxadiazolo[3,4-*b*]pyridin-7-ol (7ae). Yellow solid (31%, 67 mg) ^1H NMR (500 MHz, acetone- d_6) δ 11.54 (s, 1H), 8.29 (s, 1H), 7.29 (t, $J = 10.8$ Hz, 1H), 7.15 (dd, $J = 9.1, 7.1$ Hz, 1H), 6.72 (s, 1H). ^{19}F NMR (376 MHz, acetone- d_6) δ -61.1 (d, $J = 13.3$ Hz), -123.9, -126.8. ^{13}C NMR (126 MHz, acetone- d_6) δ 169.6, 154.6 (dd, $J = 182.9, 10.9$ Hz), 153.4, 152.8 (dd, $J = 180.7, 14.3$ Hz), 146.1, 140.7, 133.2 (d, $J = 11.4$ Hz), 123.8, 123.7 (q, $J = 273.7, 271.6, 270.5$ Hz), 113.6 (d, $J = 5.0$ Hz), 106.2 (t, $J = 24.7$ Hz). HRMS: (ESI) $[\text{M} - \text{H}]^-$ calcd for $\text{C}_{12}\text{H}_5\text{F}_5\text{N}_4\text{O}_2$ 331.0259 observed 331.0252 m/z . Δ -2.1146 ppm.

6-((5-Fluoro-2-(trifluoromethyl)phenyl)amino)-[1,2,5]oxadiazolo[3,4-*b*]pyridin-7-ol (7af). Purple solid (40%) ^1H NMR (400 MHz, acetone- d_6) δ 11.52 (s, 1H), 8.33 (d, $J = 0.7$ Hz, 1H), 7.58 (dd, $J = 6.2, 0.7$ Hz, 1H), 6.77 (dd, $J = 11.9, 0.8$ Hz, 1H), 6.65–6.56 (m, 2H). ^{13}C NMR (126 MHz, acetone- d_6) δ 169.7, 154.3 (d, $J = 245.3$ Hz), 153.4, 146.1, 141.6, 136.9 (d, $J = 11.9$ Hz), 127.3 (qd, $J = 32.2, 3.4$ Hz), 125.1 (q, $J = 271.3$ Hz), 123.3, 116.3, 116.1, 112.5 (t, $J = 4.0$ Hz). HRMS: (ESI) $[\text{M} - \text{H}]^-$ calcd for $\text{C}_{12}\text{H}_6\text{F}_4\text{N}_4\text{O}_2$, 313.0354, observed 313.0350 m/z . Δ -1.2778 ppm.

6-((3-Fluoro-5-(trifluoromethyl)phenyl)amino)-[1,2,5]oxadiazolo[3,4-*b*]pyridin-7-ol (7ag). Orange solid (24% yield, 78 mg) ^1H NMR (500 MHz, Acetone- d_6) δ 11.48 (s, 1H), 8.32 (d, $J = 0.7$ Hz, 1H), 7.22 (s, 1H), 7.03 (s, 1H), 6.86 (dt, $J = 11.5, 2.2$ Hz, 1H), 6.73 (d, $J = 8.7$ Hz, 1H). ^{19}F NMR (376 MHz, acetone- d_6) δ -63.6, -112.3 (t, $J = 10.3$ Hz). ^{13}C NMR (126 MHz, acetone- d_6) δ 169.9, 164.6 (d, $J = 242.9$ Hz), 153.6 (d, $J = 7.8$ Hz), 151.5, 151.4, 146.3, 141.6, 133.1 (dd, $J = 32.6, 10.3$ Hz), 123.7, 108.8–106.5 (m), 104.6 (d, $J = 25.8$ Hz), 102.0 (dd, $J = 25.7, 4.0$ Hz). HRMS: (ESI) $[\text{M} - \text{H}]^-$ calcd for $\text{C}_{12}\text{H}_6\text{F}_4\text{N}_4\text{O}_2$, 313.0354, observed 313.035 m/z . Δ -1.2778

6-((3-Fluoro-1,1'-biphenyl-4-yl)amino)-[1,2,5]oxadiazolo[3,4-*b*]pyridin-7-ol (7ah). Purple solid (48%, 71 mg) ^1H NMR (400 MHz, acetone- d_6) δ 8.25 (s, 1H), 7.63–7.59 (m, 2H), 7.45–7.43 (m, 1H), 7.42–7.39 (m, 2H), 7.33–7.27 (m, 2H), 7.08 (t, 1H, $J = 9.0$), 6.51 (s, 1H). ^{19}F NMR (376 MHz, acetone- d_6) δ -133.95 to -134.09 (m). ^{13}C NMR (126 MHz, acetone- d_6) δ 152.6 (d, $J = 239.8$ Hz), 152.3, 144.7, 139.7, 139.7, 136.5, 133.4 (d, $J = 11.8$ Hz), 132.4 (d, $J = 7.0$ Hz), 128.8, 126.8, 126.2, 124.3, 122.7, 122.7, 116.1, 116.1, 113.3 (d, $J = 19.9$ Hz). HRMS: (ESI) $[\text{M} - \text{H}]^-$ calcd for $\text{C}_{17}\text{H}_{11}\text{FN}_4\text{O}_2$, 321.0793, observed 321.0790 m/z . Δ -1.0278 ppm.

6-((1,1'-Biphenyl)-3-ylamino)-[1,2,5]oxadiazolo[3,4-*b*]pyridin-7-ol (7ai). Yellow solid (46%, 110 mg) ^1H NMR (500 MHz, acetone- d_6) δ 11.28 (s, 1H), 8.27 (s, 1H), 7.63–7.55 (m, 2H), 7.41 (t, $J = 7.6$ Hz, 2H), 7.32 (tt, $J = 7.7, 1.3$ Hz, 1H), 7.28 (t, $J = 1.7$ Hz, 1H), 7.26 (d, $J = 7.8$ Hz, 1H), 7.07 (ddd, $J = 7.6, 1.7, 1.0$ Hz, 1H), 7.01 (ddd, $J = 8.1, 2.3, 0.9$ Hz, 1H), 6.68 (s, 1H). ^{13}C NMR (126 MHz, acetone- d_6) δ 168.9, 152.9, 147.1, 145.4, 142.9, 142.2, 130.4, 129.5, 128.1, 127.7, 126.6, 118.9, 115.4, 114.8. HRMS: (ESI) $[\text{M} - \text{H}]^-$ calcd for $\text{C}_{17}\text{H}_{12}\text{N}_4\text{O}_2$ 303.0887 observed 303.0881 m/z . Δ -1.9796 ppm.

6-((1,1'-Biphenyl)-2-ylamino)-[1,2,5]oxadiazolo[3,4-*b*]pyridin-7-ol (7aj). Yellow solid (16%, 34 mg) ^1H NMR (500 MHz, acetone- d_6) δ 12.00 (s, 1H), 8.87 (s, 1H), 8.32 (dd, $J = 8.2, 1.4$ Hz, 2H), 8.25 (t, $J = 7.7$ Hz, 2H), 8.19–8.09 (m, 1H), 8.04–7.95 (m, 2H), 7.91 (dd, $J = 8.2, 1.2$ Hz, 1H), 7.74 (td, $J = 7.4, 1.2$ Hz, 1H), 6.82 (s, 1H). ^{13}C NMR (126 MHz, acetone- d_6) δ 168.6, 152.8, 145.0, 142.7, 140.2,

134.0, 131.5, 130.0, 129.7, 129.2, 128.2, 127.0, 121.3, 116.6. HRMS: (ESI) $[M - H]^-$ calcd for $C_{17}H_{12}N_4O_2$ 303.0887 observed 303.0885 m/z . Δ -0.6599 ppm.

6-((2'-Fluoro-[1,1'-biphenyl]-4-yl)amino)-[1,2,5]oxadiazolo[3,4-b]pyridin-7-ol (**7ak**). Orange solid (40%, 83 mg) 1H NMR (500 MHz, acetone- d_6) δ 11.31 (s, 1H), 8.27 (s, 1H), 7.48 (td, J = 7.9, 1.9 Hz, 1H), 7.41 (dd, J = 8.7, 1.8 Hz, 2H), 7.32 (dddd, J = 8.1, 7.0, 5.0, 1.8 Hz, 1H), 7.24 (dd, J = 7.5, 1.3 Hz, 1H), 7.23–7.15 (m, 1H), 7.12–7.02 (m, 2H), 6.75 (s, 1H). ^{19}F NMR (376 MHz, acetone- d_6) δ -119.7. ^{13}C NMR (126 MHz, acetone- d_6) δ 160.6 (d, J = 245.1 Hz), 153.1, 146.6, 145.5, 136.3, 131.2 (d, J = 3.7 Hz), 130.5 (d, J = 3.2 Hz), 129.8 (d, J = 13.1 Hz), 129.1 (d, J = 8.3 Hz), 127.1, 126.1, 125.5 (d, J = 3.6 Hz), 116.7 (d, J = 23.0 Hz), 115.9. HRMS: (ESI) $[M - H]^-$ calcd for $C_{17}H_{11}FN_4O_2$, 323.09388, observed 323.0942 m/z . Δ 0.9904 ppm.

6-((3'-Fluoro-[1,1'-biphenyl]-4-yl)amino)-[1,2,5]oxadiazolo[3,4-b]pyridin-7-ol (**7al**). Purple solid (25%, 53 mg) 1H NMR (500 MHz, acetone- d_6) δ 11.33 (s, 1H), 8.26 (s, 1H), 7.53 (d, J = 8.7 Hz, 2H), 7.46–7.40 (m, 2H), 7.34 (ddt, J = 10.5, 2.1, 1.1 Hz, 1H), 7.13–7.05 (m, 2H), 7.06–6.97 (m, 1H), 6.77 (s, 1H). ^{19}F NMR (376 MHz, acetone- d_6) δ -114.9. ^{13}C NMR (126 MHz, acetone- d_6) δ 164.2 (d, J = 243.0 Hz), 153.1, 147.0, 145.5, 144.4 (d, J = 8.0 Hz), 136.6, 131.3 (d, J = 8.6 Hz), 131.0 (d, J = 2.3 Hz), 128.5, 126.0, 122.7 (d, J = 2.5 Hz), 116.3, 113.6 (d, J = 21.4 Hz), 113.3 (d, J = 22.2 Hz). HRMS: (ESI) $[M - H]^-$ calcd for $C_{17}H_{11}FN_4O_2$, 323.09388, observed 323.0953 m/z . Δ 4.6426 ppm.

6-((3'-Chloro-[1,1'-biphenyl]-4-yl)amino)-[1,2,5]oxadiazolo[3,4-b]pyridin-7-ol (**7am**). Purple Solid (9%, 19 mg) 1H NMR (400 MHz, acetone- d_6) δ 11.30 (s, 1H), 8.28–8.23 (m, 1H), 7.61–7.58 (m, 1H), 7.57–7.49 (m, 3H), 7.41 (td, J = 7.9, 0.4 Hz, 1H), 7.28 (ddd, J = 7.9, 2.1, 1.0 Hz, 1H), 7.09 (d, J = 8.7 Hz, 1H), 6.77 (s, 1H). ^{13}C NMR (126 MHz, acetone- d_6) δ 153.0, 147.1, 145.5, 144.0, 136.5, 135.1, 131.2, 130.8, 128.5, 126.9, 126.7, 125.9 (d, J = 8.6 Hz), 125.4, 116.3, 116.3. HRMS: (ESI) $[M - H]^-$ calcd for $C_{17}H_{11}ClN_4O_2$, 337.0497, observed 337.0492 m/z . Δ -1.4834 ppm.

6-((3'-Trifluoromethyl)-[1,1'-biphenyl]-4-yl)amino)-[1,2,5]oxadiazolo[3,4-b]pyridin-7-ol (**7an**). Purple solid (33%, 82 mg) 1H NMR (500 MHz, acetone- d_6) δ 11.34 (s, 1H), 8.27 (s, 1H), 7.95–7.83 (m, 2H), 7.67–7.43 (m, 4H), 7.10 (d, J = 8.7 Hz, 2H), 6.80 (s, 1H). ^{19}F NMR (376 MHz, acetone- d_6) δ -63.1. ^{13}C NMR (126 MHz, acetone- d_6) δ 153.1, 147.3, 145.6, 142.9, 136.8, 131.4 (d, J = 31.6 Hz), 130.6 (d, J = 3.6 Hz), 130.5, 128.6, 125.9, 125.5 (d, J = 271.5 Hz), 123.4 (dd, J = 37.7, 4.0 Hz), 116.3. HRMS: (ESI) $[M + H]^+$ calcd for $C_{18}H_{11}F_3N_4O_2$ 373.0906 observed 373.0918 m/z . Δ 3.2163 ppm.

6-((4'-Fluoro-[1,1'-biphenyl]-4-yl)amino)-[1,2,5]oxadiazolo[3,4-b]pyridin-7-ol (**7ao**). Purple solid (17%, 34 mg) 1H NMR (400 MHz, acetone- d_6) δ 11.31 (s, 1H), 8.24 (s, 1H), 7.61 (dd, J = 8.9, 5.4 Hz, 2H), 7.48 (d, J = 8.7 Hz, 2H), 7.16 (t, J = 8.9 Hz, 2H), 7.09 (d, J = 8.7 Hz, 1H), 6.70 (s, 1H). ^{19}F NMR (376 MHz, acetone- d_6) δ -118.9. ^{13}C NMR (126 MHz, acetone- d_6) δ 162.7 (d, J = 243.3 Hz), 152.9, 146.3, 145.4, 138.3, 135.5, 131.7, 128.7 (d, J = 7.9 Hz), 128.3, 126.4, 116.5, 116.2 (d, J = 21.4 Hz). HRMS: (ESI) $[M - H]^-$ calcd for $C_{17}H_{11}FN_4O_2$ 321.0793 observed 321.0791 m/z . Δ -0.6228 ppm.

6-((4'-Chloro-[1,1'-biphenyl]-4-yl)amino)-[1,2,5]oxadiazolo[3,4-b]pyridin-7-ol (**7ap**). Purple solid (42%, 1.98 g) 1H NMR (400 MHz, acetone- d_6) δ 11.31 (s, 1H), 8.23 (s, 1H), 7.60 (d, J = 8.5 Hz, 2H), 7.49 (d, J = 8.5 Hz, 3H), 7.41 (d, J = 8.5 Hz, 3H), 7.07 (d, J = 8.7 Hz, 3H), 6.72 (s, 1H). ^{13}C NMR (126 MHz, acetone- d_6) δ 169.26, 153.00, 146.85, 145.58, 140.68, 136.12, 132.56, 131.12, 129.66, 128.53, 128.41, 126.19, 116.40. HRMS: ESI $[M - H]^-$ calc for $C_{17}H_{11}ClN_4O_2$, 339.0643, observed, 339.0646. m/z . Δ 0.8847 ppm.

6-((4'-Trifluoromethyl)-[1,1'-biphenyl]-4-yl)amino)-[1,2,5]oxadiazolo[3,4-b]pyridin-7-ol (**7aq**). Purple solid (30%, 73 mg) 1H NMR (400 MHz, acetone- d_6) δ 11.33 (s, 1H), 8.27 (d, J = 0.6 Hz, 1H), 7.86–7.78 (m, 2H), 7.73 (d, J = 8.6 Hz, 2H), 7.58 (d, J = 8.7 Hz, 2H), 7.10 (d, J = 8.8 Hz, 1H), 6.82 (s, 1H). ^{19}F NMR (376 MHz, acetone- d_6) δ -62.8. ^{13}C NMR (126 MHz, acetone- d_6) δ 169.1, 153.1, 147.6, 145.6 (d, J = 16.8 Hz), 137.0, 130.5, 128.7, 128.4 (d, J = 31.9 Hz), 127.3, 126.5 (d, J = 4.0 Hz), 125.8, 125.7, 125.6 (d, J =

271.1 Hz), 116.2. HRMS: (ESI) $[M + H]^+$ calcd for $C_{18}H_{11}F_3N_4O_2$ 373.0907 observed 373.0906 m/z . Δ -0.2680 ppm.

6-((4-(6-Trifluoromethyl)pyridin-3-yl)phenyl)amino)-[1,2,5]oxadiazolo[3,4-b]pyridin-7-ol (**7ar**). Purple solid (42%, 71 mg) 1H NMR (400 MHz, acetone) δ 11.5 (s, 1H), 8.97 (dt, J = 2.3, 0.7 Hz, 1H), 8.29 (s, 1H), 8.26–8.18 (m, 1H), 7.84 (dd, J = 8.3, 0.8 Hz, 1H), 7.68–7.59 (m, 2H), 7.15–7.07 (m, 2H), 6.91 (s, 1H). ^{19}F NMR (376 MHz, acetone) δ -68.06. ^{13}C NMR (126 MHz, acetone) δ 169.3, 153.2, 148.5, 148.4, 145.8, 145.7 (q, J = 34.2 Hz), 140.3, 138.2, 135.2, 129.0, 126.9, 125.2, 123.1 (q, J = 272.8 Hz), 121.4 (d, J = 3.0 Hz), 116.1. HRMS: (ESI) $[M + H]^+$ calcd for $C_{17}H_{10}F_3N_5O_2$ 374.0859 observed 374.0861 m/z . Δ 0.5346

6-((2',3'-Difluoro-[1,1'-biphenyl]-4-yl)amino)-[1,2,5]oxadiazolo[3,4-b]pyridin-7-ol (**7as**). Purple solid (17%, 36 mg) 1H NMR (400 MHz, acetone- d_6) δ 10.58 (s, 1H), 8.28 (s, 1H), 7.42 (dd, J = 8.7, 1.8 Hz, 2H), 7.33–7.25 (m, 1H), 7.25–7.19 (m, 2H), 7.11–7.02 (m, 2H), 6.82 (s, 1H). ^{19}F NMR (376 MHz, acetone d_6) δ -140.5, -146.3. ^{13}C NMR (126 MHz, acetone- d_6) δ 169.0, 159.1, 153.2, 151.9 (dd, J = 245.1, 13.5 Hz), 148.5 (dd, J = 246.5, 13.0 Hz), 147.4, 145.6, 137.4, 132.2 (d, J = 10.0 Hz), 130.6 (d, J = 3.4 Hz), 129.6 (d, J = 72.4 Hz), 126.0, 125.7 (d, J = 8.2 Hz), 125.4 (dd, J = 7.5, 4.9 Hz), 118.7, 115.9 (d, J = 17.5 Hz), 115.7. HRMS: (ESI) $[M + H]^+$ calcd for $C_{17}H_{10}F_2N_4O_2$, 341.0844 observed 341.0850 m/z . Δ 1.7591 ppm.

6-((2',3'-Dichloro-[1,1'-biphenyl]-4-yl)amino)-[1,2,5]oxadiazolo[3,4-b]pyridin-7-ol (**7at**). Purple solid (28%, 67 mg) 1H NMR (500 MHz, acetone- d_6) δ 11.35 (s, 1H), 8.28 (s, 1H), 7.53 (dd, J = 7.9, 1.7 Hz, 1H), 7.37 (t, J = 7.5 Hz, 1H), 7.33 (dd, J = 7.7, 1.7 Hz, 1H), 7.27 (d, J = 8.6 Hz, 2H), 7.06 (d, J = 8.6 Hz, 2H), 6.78 (s, 1H). ^{13}C NMR (126 MHz, acetone- d_6) δ 168.8, 153.2, 147.1, 145.6, 144.0, 137.4, 133.8, 131.3, 131.0, 130.8, 130.4, 129.7, 128.7, 125.8, 115.2. HRMS: (ESI) $[M - H]^-$ calcd for $C_{17}H_{10}Cl_2N_4O_2$, 371.0108, observed 371.0104 m/z . Δ -1.0781 ppm.

6-((3',4'-Difluoro-[1,1'-biphenyl]-4-yl)amino)-[1,2,5]oxadiazolo[3,4-b]pyridin-7-ol (**7au**). Purple solid (37%, 81 mg) 1H NMR (500 MHz, acetone- d_6) δ 11.36 (s, 1H), 8.25 (s, 1H), 7.56–7.46 (m, 3H), 7.41 (dddd, J = 8.6, 4.4, 2.3, 1.3 Hz, 1H), 7.33 (dt, J = 10.6, 8.5 Hz, 1H), 7.07 (d, J = 8.7 Hz, 2H), 6.77 (s, 1H). ^{19}F NMR (376 MHz, acetone- d_6) δ -140.1, -143.1 to -144.9 (m). ^{13}C NMR (126 MHz, acetone- d_6) δ 169.1, 153.0, 151.5 (dd, J = 172.3, 12.8 Hz), 149.5 (dd, J = 172.3, 12.9 Hz), 147.0, 145.5, 139.5 (dd, J = 6.1, 3.7 Hz), 136.6, 130.2, 128.4, 126.0, 123.2 (dd, J = 6.1, 3.3 Hz), 118.3 (d, J = 17.2 Hz), 116.3, 115.5 (d, J = 17.7 Hz). HRMS: (ESI) $[M - H]^+$ calcd for $C_{17}H_{10}F_2N_4O_2$, 341.0847, observed 341.0853 m/z . Δ 1.7590 ppm.

6-((2',5'-Difluoro-[1,1'-biphenyl]-4-yl)amino)-[1,2,5]oxadiazolo[3,4-b]pyridin-7-ol (**7av**). Purple solid (10%, 22 mg) 1H NMR (500 MHz, acetone- d_6) δ 11.33 (s, 1H), 8.28 (s, 1H), 7.44 (dd, J = 8.7, 1.8 Hz, 2H), 7.32–7.17 (m, 2H), 7.08 (d, J = 8.8 Hz, 3H), 6.81 (s, 1H). ^{19}F NMR (376 MHz, acetone- d_6) δ -120.3 to -121.0 (m), -125.4 (dd, J = 10.2, 8.2 Hz). ^{13}C NMR (126 MHz, acetone- d_6) δ 159.8 (d, J = 239.9 Hz), 156.7 (d, J = 240.4 Hz), 153.1, 147.4, 145.6, 137.0, 131.5, 130.5 (d, J = 3.8 Hz), 125.8, 118.1 (dd, J = 26.5, 9.1 Hz), 116.9 (dd, J = 24.4, 4.2 Hz), 115.7, 115.0 (dd, J = 24.3, 8.7 Hz). HRMS: (ESI) $[M + H]^+$ calcd for $C_{17}H_{10}F_2N_4O_2$ 341.0844 observed 341.0857 m/z . Δ 3.8114 ppm.

6-((3',5'-Bis(trifluoromethyl)-[1,1'-biphenyl]-4-yl)amino)-[1,2,5]oxadiazolo[3,4-b]pyridin-7-ol (**7aw**). Purple solid (44%, 127 mg) 1H NMR (500 MHz, acetone- d_6) δ 11.42 (s, 1H), 8.29 (s, 2H), 8.19 (d, J = 1.8 Hz, 2H), 7.92–7.87 (m, 1H), 7.69 (d, J = 8.7 Hz, 2H), 7.11 (d, J = 8.6 Hz, 2H), 6.91 (s, 1H). ^{19}F NMR (376 MHz, acetone- d_6) δ -63.4. ^{13}C NMR (126 MHz, acetone- d_6) δ 153.2, 148.4, 145.7, 144.4, 138.0, 132.5 (d, J = 33.0 Hz), 129.0, 128.6, 127.0, 125.4, 124.6 (d, J = 272.0 Hz), 120.2, 116.1. HRMS: (ESI) $[M + H]^+$ calcd for $C_{19}H_{10}F_6N_4O_2$ 441.0780 observed 441.0778 m/z . Δ -0.4534 ppm.

6-(Naphthalen-2-ylamino)-[1,2,5]oxadiazolo[3,4-b]pyridin-7-ol (**7ax**). Purple solid (23%, 56 mg) 1H NMR (500 MHz, acetone- d_6) δ 11.32 (s, 1H), 8.34 (s, 1H), 7.83–7.68 (m, 2H), 7.59 (dd, J = 8.4, 1.1 Hz, 1H), 7.38–7.32 (m, 2H), 7.30 (d, J = 2.3 Hz, 1H), 7.22 (ddd, J = 8.1, 6.8, 1.2 Hz, 1H), 6.80 (s, 1H). ^{13}C NMR (126 MHz, acetone- d_6) δ 168.9, 153.0, 145.4, 144.5, 135.8, 129.8, 129.5, 128.4, 127.0, 126.4,

123.5, 119.9, 109.0. HRMS: (ESI) $[M + H]^+$ calcd for $C_{15}H_{10}N_4O_2$ 279.0877 observed 279.0878 m/z . Δ 0.3583 ppm.

6-((9,9-Dimethyl-9H-fluoren-2-yl)amino)-[1,2,5]oxadiazolo[3,4-*b*]pyridin-7-ol (**7ay**). Red solid (50%, 150 mg) 1H NMR (400 MHz, acetone- d_6) δ 11.21 (s, 1H), 8.25 (s, 1H), 7.67–7.58 (m, 2H), 7.43 (d, $J = 7.3$ Hz, 1H), 7.30–7.17 (m, 3H), 7.01 (dd, $J = 8.2, 2.1$ Hz, 1H), 6.69 (s, 1H), 1.43 (s, 6H). ^{13}C NMR (126 MHz, acetone- d_6) δ 156.1, 153.8, 152.8, 146.1, 145.2, 140.4, 134.2, 131.9, 127.7, 127.0, 126.6, 123.2, 121.5, 119.6, 115.5, 111.2, 47.3, 27.5. HRMS: (ESI) $[M + H]^+$ calcd for $C_{20}H_{16}N_4O_2$ 345.1346 observed 345.1345 m/z . Δ -0.2897 ppm.

6-Bromo-[1,2,5]oxadiazolo[3,4-*b*]pyridin-7-ol (**8**). 6-Bromo-7-methoxy-[1,2,5]oxadiazolo[3,4-*b*]pyridine (500 mg, 2.2 mmol) and NaOH (260 mg, 6.5 mmol) were dissolved in dioxane (0.5 mL) and water (0.5 mL). The reaction was stirred for 15 min at room temperature. The reaction mixture was diluted with water, acidified with 10% aq. HCl and extracted with ethyl acetate (3 times). The organic extracts were combined, dried with anhydrous sodium sulfate, filtered, and concentrated *in vacuo* to afford **8** as a crude yellow amorphous solid. HRMS: (ESI) $[M - H]^+$ calcd for $C_6H_4BrN_3O_2$ 215.9403, observed 215.9405 m/z . Δ 0.9262 ppm.

General Suzuki Procedure for h. To a sealed vial containing Pd(dppf) $Cl_2 \cdot CH_2Cl_2$ (0.1 equiv), 6-bromo-[1,2,5]oxadiazolo[3,4-*b*]pyridin-7-ol (**8**) (1.00 equiv), boronic acid (1.1 equiv), and $NaCO_3$ (2.5 equiv) was added 1,4-dioxane (0.1 M) and water (0.1 M) under a nitrogen atmosphere. The reaction was heated to 90 °C for 16 h. The reaction mixture was allowed to cool to room temperature, acidified with 10% aq. HCl and extracted with ethyl acetate (3 times). The organic extracts were combined, dried with anhydrous sodium sulfate, filtered, concentrated *in vacuo*, and purified via chromatography on SiO_2 (solvent system: ethyl acetate/hexanes) to afford the desired products **9**. Yields are listed as combined over two steps.

6-(2-Fluorophenyl)-[1,2,5]oxadiazolo[3,4-*b*]pyridin-7-ol (**9a**). Yellow solid (7%, 10 mg) 1H NMR (400 MHz, acetone- d_6) δ 11.61 (s, 1H), 8.20 (d, $J = 0.9$ Hz, 1H), 7.49 (td, $J = 7.5, 1.8$ Hz, 1H), 7.42 (dddd, $J = 8.2, 7.2, 5.2, 1.8$ Hz, 1H), 7.26 (dd, $J = 7.5, 1.2$ Hz, 1H), 7.23–7.17 (m, 1H). ^{19}F NMR (376 MHz, acetone- d_6) δ -111.7 to -117.6 (m). ^{13}C NMR (126 MHz, acetone- d_6) δ 170.4, 161.4 (d, $J = 246.6$ Hz), 153.7, 145.8, 143.7, 133.1, 130.6, 124.9, 118.5, 116.3 (d, $J = 22.7$ Hz). HRMS: (ESI) $[M - H]^+$ calcd for $C_{11}H_6FN_3O_2$ 323.0516, observed 323.0526 m/z . Δ 3.0954 ppm.

6-(2-Chlorophenyl)-[1,2,5]oxadiazolo[3,4-*b*]pyridin-7-ol (**9b**). Yellow solid (20%, 45 mg) 1H NMR (600 MHz, acetone- d_6) δ 11.64 (s, 1H), 8.12 (s, 1H), 7.51–7.50 (m, 1H), 7.40–7.39 (m, 3H). ^{13}C NMR (151 MHz, acetone- d_6) δ 170.3, 153.7, 145.8, 143.8, 135.3, 134.1, 133.6, 130.5, 130.2, 127.7, 122.3. HRMS: (ESI) $[M + H]^+$ calcd for $C_{11}H_6ClN_3O_2$ 248.0221 observed 248.0233 m/z . Δ 4.8383 ppm.

6-(3-Chlorophenyl)-[1,2,5]oxadiazolo[3,4-*b*]pyridin-7-ol (**9c**). Yellow solid, (31%, 70 mg) 1H NMR (600 MHz, acetone- d_6) δ 11.72 (s, 1H), 8.34 (s, 1H), 7.69 (t, $J = 1.9$ Hz, 1H), 7.58 (ddd, $J = 7.7, 1.7, 1.0$ Hz, 1H), 7.44 (t, $J = 7.9$ Hz, 1H), 7.37 (ddd, $J = 8.0, 2.1, 1.0$ Hz, 2H). ^{13}C NMR (151 MHz, acetone- d_6) δ 170.9, 153.5, 146.1, 143.4, 137.1, 134.3, 130.7, 129.5, 128.1, 128.1, 121.9. HRMS: (ESI) $[M + H]^+$ calcd for $C_{11}H_6ClN_3O_2$ 248.0221, observed 248.0227 m/z . Δ 2.4191 ppm.

6-(3-(Trifluoromethyl)phenyl)-[1,2,5]oxadiazolo[3,4-*b*]pyridin-7-ol (**9d**). Yellow solid (26%, 67 mg) 1H NMR (600 MHz, acetone- d_6) δ 11.75 (s, 1H), 8.42 (s, 1H), 7.99 (s, 1H), 7.90 (d, $J = 7.4$ Hz, 2H), 7.65 (m, 3H). ^{19}F NMR (565 MHz, acetone- d_6) δ -63.0. ^{13}C NMR (151 MHz, acetone- d_6) δ 171.0, 153.5, 146.1, 143.8, 136.0, 133.4, 130.7 (q, $J = 32.0$ Hz), 129.9, 126.2 (q, $J = 3.7$ Hz), 124.8 (q, $J = 3.9$ Hz), 124.4, 121.8. HRMS: (ESI) $[M + H]^+$ calcd for $C_{12}H_6F_3N_3O_2$ 282.0485 observed 282.0498 m/z . Δ 4.6446 ppm.

6-(4-Chlorophenyl)-[1,2,5]oxadiazolo[3,4-*b*]pyridin-7-ol (**9e**). Yellow solid (32%, 92 mg) 1H NMR (500 MHz, acetone- d_6) δ 11.66 (s, 1H), 8.30 (s, 1H), 7.65 (d, $J = 8.6$ Hz, 2H), 7.44 (d, $J = 8.6$ Hz, 2H). ^{13}C NMR (126 MHz, acetone- d_6) δ 170.9, 153.5, 146.1, 143.0, 133.8, 133.5, 131.3, 129.0, 122.1. HRMS: (ESI) $[M + H]^+$

calcd for $C_{11}H_6ClN_3O_2$ 248.0221, observed 248.0226 m/z . Δ 2.0159 ppm.

6-(4-(Trifluoromethoxy)phenyl)-[1,2,5]oxadiazolo[3,4-*b*]pyridin-7-ol (**9f**). Yellow solid (34%, 94 mg) 1H NMR (600 MHz, acetone- d_6) δ 11.75 (s, 1H), 8.39 (s, 1H), 7.70–7.66 (m, 1H), 7.60–7.56 (m, 1H), 7.31–7.30 (m, 1H). ^{19}F NMR (565 MHz, acetone- d_6) δ -58.4. ^{13}C NMR (126 MHz, acetone- d_6) δ 170.9, 153.5, 149.8, 146.2, 143.6, 137.3, 130.7, 128.4, 122.3, 121.7, 121.5 (q, $J = 255.5$ Hz), 120.6. HRMS: (ESI) $[M + H]^+$ calcd for $C_{12}H_6F_3N_3O_3$ 298.0434 observed 298.0448 m/z . Δ 4.6973 ppm.

6-(Thiophen-2-yl)-[1,2,5]oxadiazolo[3,4-*b*]pyridin-7-ol (**9g**). Yellow solid (13%, 24 mg). 1H NMR (600 MHz, acetone- d_6) δ 8.70 (s, 1H), 7.58 (dd, $J = 3.7, 1.1$ Hz, 1H), 7.43 (dd, $J = 5.1, 1.2$ Hz, 1H), 7.01 (dd, $J = 5.1, 3.7$ Hz, 1H). ^{13}C NMR (151 MHz, acetone- d_6) δ 169.3, 153.6, 145.7, 142.4, 136.0, 127.0, 125.9, 123.8, 117.4. HRMS: (ESI) $[M + H]^+$ calcd for $C_9H_5N_3O_2S$ 220.0175 observed 220.0178 m/z . Δ 1.3635 ppm.

6-(4'-Fluoro-[1,1'-biphenyl]-4-yl)-[1,2,5]oxadiazolo[3,4-*b*]pyridin-7-ol (**9h**). Yellow solid (11%, 23 mg) 1H NMR (400 MHz, acetone- d_6) δ 11.61 (s, 1H), 8.32 (s, 1H), 7.89–7.57 (m, 6H), 7.32–7.11 (m, 2H). ^{19}F NMR (376 MHz, acetone- d_6) δ -117.3. ^{13}C NMR (126 MHz, acetone- d_6) δ 171.1, 163.4 (d, $J = 244.7$ Hz), 153.6, 146.2, 142.8, 139.7, 137.8 (d, $J = 3.2$ Hz), 134.2, 129.6 (d, $J = 8.1$ Hz), 127.4, 122.9, 116.5 (d, $J = 21.5$ Hz). HRMS: (ESI) $[M + H]^+$ calcd for $C_{17}H_{10}FN_3O_2$ 308.0829 observed 308.0841 m/z . Δ 3.8950 ppm.

OCR Seahorse Assay. OCR was measured using an Agilent Seahorse XF24 or XFe96 Analyzer (Agilent Technologies, Santa Clara, CA). L6 myoblasts were seeded in a Seahorse 24 or 96-well tissue culture plate at a density of 3.5×10^4 cells/well. The cells were then allowed to adhere overnight. Prior to the assay, the media was changed to unbuffered Dulbecco's modified Eagle's medium (DMEM) containing pyruvate and glutamine (Gibco no. 12800-017, pH = 7.4 at 37 °C), and the cells were equilibrated for 1 h at 37 °C without CO_2 . Compounds were injected during the assay, and OCR was measured using 2 min measurement periods. Cells were treated with a single drug concentration per well and measured over a 90 min period. Two wells were used per condition and, where applicable, results from multiple plates were averaged together. The first three measurements after injection for each concentration were averaged to produce a dose curve. EC_{50} values were calculated using the GraphPad Prism's nonlinear regression built-in equation, $Y = Bottom + (\hat{X}Hillslope) \times (Top - Bottom) / (\hat{X}HillSlope + EC_{50}HillSlope)$, with the Bottom constrained to the 100% baseline. AUC values were also calculated using the same software.

Pharmacokinetics Protocol. Pharmacokinetics assessment was performed in 8-weeks-old male C57BL/6 mice by oral gavage at a dose of 10 mg/kg of body weight. The compound was delivered in a mixture containing 99.8% (v/v) methylcellulose (0.5% solution made in water, Sigma, M0512) and 0.2% (v/v) Tween 80 (Sigma, P6474), obtained via solubilizing the drug into a Potter Elvehjem tissue homogenizer. Blood collection was performed at the indicated time points from a tail nick with a razor blade into lithium heparin-coated Microvette CB 300 tubes (Sarstedt, 16.443). Samples were processed at UNSW for liquid chromatography tandem mass spectrometry (LC-MS/MS) by protein precipitation into a mixture of acetonitrile/methanol solution (AcN-MeOH, 9:1). Seven μL of plasma was precipitated in 100 μL of AcN-MeOH, followed by centrifugation at 18,000g for 10 min and collection of the supernatant for analysis. Standards were prepared by spiking known concentrations (1–250 ng/ μL) of **SHO1122147** into plasma samples from untreated mice. LC-MS/MS was performed on a Shimadzu Prominence LCMS-8030 instrument (Shimadzu, Japan). Chromatographic separation was achieved using an ACUITY UPLC BEH, C18 column (Waters, WT186002350, USA). Mobile phase A consisted of 0.1% v/v formic acid in HPLC grade water, while mobile phase B consisted of 0.1% v/v formic acid in ACN. Electrospray ionization (ESI) was performed in negative mode. Elution was achieved with a gradient of 20–100% mobile phase B at a flow rate of 0.4 mL/min with 10 μL injection volume electro-sprayed into the mass spectrometer. Transitions of m/z 336.9 > 320 and 336.9 > 336.9 with a 4.29 min retention time were

used. Pharmacokinetic properties were calculated using PKSolver add-in tool (Excel).

For the no observed adverse effect level (NOAEL) study, 9-week-old male C57BL/6 mice received either vehicle or **SHO1122147** (30, 100, 300, 1000 mg/kg of body weight) by oral gavage and were carefully monitored for 24 h after dosing. Core body temperature was measured with a rectal probe thermometer (Braintree, TW2–107) at the time points shown. Food intake and body weight were also recorded over time, and no signs of discomfort or ill-thrift were observed.

Gubra-Amylin NASH (GAN) Animal Study. Animal experiments performed at UNSW were approved by the Animal Care and Ethics Committee (animal ethics approval #20/67A). C57BL/6 male mice were purchased from Australian BioResources (Moss Vale, NSW, Australia) and group-housed at 22 °C in a light-dark cycle of 12 h. Mice were provided with ad libitum access to water and normal chow diet (Gordons Specialty Feeds, NSW, Australia). We first conditioned 5/6-week-old mice on GAN diet for 33 weeks. Gubra-Amylin NASH (GAN) diet was prepared in-house and was adapted from Research Diets #D09100310: caloric content was distributed as 46% fat kcal (of which 15% were palm oil by weight), 36% sugar (of which 22% fructose and 10% sucrose by weight) and 18% protein. Diet ingredients were purchased from local suppliers. For diet preparation, we used: palm oil (MOI Foods (M) Sdn Bhd), fructose (Food Ingredients Depot, F04230), cholesterol (Sigma, C8503, 2% by weight), sucrose (JL Stewart, GRAD25B), corn starch (JL Stewart, CFLR25W), wheat bran (JL Stewart, BRAN10UF), casein (Cottee Group, NA), choline bitartrate (Sigma, C1629), lard (JL Stewart, LARD15), soybean oil (Masterol Foods, 165194538), trace minerals (MP Biomedicals, 0296026401), AIN-93 M mineral mix (MP Biomedicals, 0296040102) and AIN-93-VX vitamin mix (MP Biomedicals, 0296040201). One week before treatment, mice were single housed and stratified into groups using baseline body weight and body composition measurements to ensure similar starting parameters. Once stratified, mice were fed either GAN diet alone or GAN diet mixed with **SHO1122147** for 4 weeks; **SHO1122147**-treated mice received fresh compound daily at 200 mg/kg of body weight. Body weight and food intake were measured daily throughout the treatment period. All mice were assessed for body composition on a weekly basis during treatment period by EchoMRI. On the final day of the study, mice were anesthetized with isoflurane and exsanguinated by cardiac puncture, and harvested tissues were frozen in liquid nitrogen prior to storage at –80 °C.

Biochemical Assays. Lipids from liver tissue were extracted using a modified version of Folch et al.'s (1957) method. Briefly, liver lipids were extracted from approximately 20 mg of tissue with 2:1 chloroform–methanol (v/v), following two washing steps of the lipid-rich lower phase in saline. Liver lipid extracts were dried under a steady stream of nitrogen in a TurboVap evaporator (Biotage) and were resuspended in 0.4 mL of 95% ethanol. Following 10 min of heating at 37 °C, lipid extracts were used to test triglycerides and cholesterol content using colorimetric assays (Pointe Scientific #T7532 and Thermo Scientific # TR13421), following manufacturer's instructions. The results obtained were normalized to initial grams/sample extracted. Plasma alanine aminotransferase (ALT) activity was measured in ethylenediamine tetraacetic acid (EDTA) plasma samples collected at the end of the study using ALT Activity Assay (Sigma, #MAK052) following manufacturer's instructions; samples were diluted 1:8 in ALT Assay Buffer.

Liver Histology and NAFLD Score. Formalin-fixed liver samples were paraffin-embedded, sectioned, and stained with hematoxylin-eosin and picosirius red. The NAFLD activity score (NAS) system was applied to all samples for scoring of steatosis, lobular inflammation and hepatocyte ballooning, and fibrosis stage was assigned as outlined by Kleiner et al., Hepatology 2005. Histological analyses were analyzed by PathCelerate Ltd. (Goostrey, Cheshire, UK); all assessments were performed by a pathologist blind to treatment.

Statistical Analysis. All data are presented as the mean ± standard error of the mean (SEM). Statistical testing was carried out

using Prism (v.10.2.0; GraphPad Software), where the threshold for significance was designated as $p < 0.05$, compared to controls. For normally distributed data, differences between groups were examined using analysis of variance (ANOVA) with Dunnett's *post hoc* test for multiple comparisons. For nonparametric data, the Kruskal–Wallis test was conducted with Dunn's *post hoc* test for multiple comparisons.

■ ASSOCIATED CONTENT

SI Supporting Information

The Supporting Information is available free of charge at <https://pubs.acs.org/doi/10.1021/acs.jmedchem.4c02366>.

Molecular formula strings (CSV)

UPLC of **7ao**, **7ap**, **7al**, and **7m** as well as ^1H , ^{13}C NMR, and HRMS of **7m** (**SHO1122147**) (PDF)

■ AUTHOR INFORMATION

Corresponding Authors

Kyle L. Hoehn – School of Biotechnology and Biomolecular Sciences, University of New South Wales, Kensington, NSW 2033, Australia; Departments of Pharmacology and Medicine, University of Virginia, Charlottesville, Virginia 22908, United States; Email: k.hoehn@unsw.edu.au

Webster L. Santos – Department of Chemistry and Virginia Tech Center for Drug Discovery, Virginia Tech, Blacksburg, Virginia 24061, United States; orcid.org/0000-0002-4731-8548; Email: santosw@vt.edu

Authors

Mary A. Foutz – Department of Chemistry and Virginia Tech Center for Drug Discovery, Virginia Tech, Blacksburg, Virginia 24061, United States

Emily L. Krinos – Department of Chemistry and Virginia Tech Center for Drug Discovery, Virginia Tech, Blacksburg, Virginia 24061, United States

Martina Beretta – School of Biotechnology and Biomolecular Sciences, University of New South Wales, Kensington, NSW 2033, Australia

Stefan R. Hargett – Departments of Pharmacology and Medicine, University of Virginia, Charlottesville, Virginia 22908, United States

Riya Shrestha – School of Biotechnology and Biomolecular Sciences, University of New South Wales, Kensington, NSW 2033, Australia

Jacob H. Murray – Department of Chemistry and Virginia Tech Center for Drug Discovery, Virginia Tech, Blacksburg, Virginia 24061, United States

Ethan Duerre – Department of Chemistry and Virginia Tech Center for Drug Discovery, Virginia Tech, Blacksburg, Virginia 24061, United States

Joseph M. Salamoun – Department of Chemistry and Virginia Tech Center for Drug Discovery, Virginia Tech, Blacksburg, Virginia 24061, United States

Katrina McCarter – Department of Chemistry and Virginia Tech Center for Drug Discovery, Virginia Tech, Blacksburg, Virginia 24061, United States

Divya P. Shah – School of Biotechnology and Biomolecular Sciences, University of New South Wales, Kensington, NSW 2033, Australia

Complete contact information is available at:

<https://pubs.acs.org/10.1021/acs.jmedchem.4c02366>

Author Contributions

The manuscript was written through contributions of all authors. All authors have given approval to the final version of the manuscript.

Notes

The authors declare the following competing financial interest(s): W.L.S. and K.L.H. are inventors of small molecule mitochondrial uncouplers that are licensed to Uncoupler Biosciences, Inc.

ACKNOWLEDGMENTS

We thank NIH (R01DK128612) for funding. EchoMRI data presented in this work was acquired using instruments at the Biological Resources Imaging Laboratory; LC-MS/MS data was acquired using instruments at the Bioanalytical Mass Spectrometry Facility; histological data was acquired at the Katharina Gaus Light Microscopy Facility; these facilities are parts of the Mark Wainwright Analytical Centre, which is in part funded by the Research Infrastructure Program of UNSW (Sydney).

ABBREVIATIONS USED

ATP, adenosine triphosphate; BMI, body mass index; DNP, 2,4-dinitrophenol; GAN, Gubra-Amylin MASH; GIP, glucose dependent insulinotropic polypeptide; GLP-1, glucagon-like peptide 1; MAFLD, metabolic-associated fatty liver disease; MASH, metabolic dysfunction-associated steatohepatitis; OCR, oxygen consumption rate; PO, *per oral*; PMF, proton motive force; ROS, reactive oxygen species; SAR, structure activity relationship; UCPS, uncoupling proteins

REFERENCES

- (1) Lustig, R. H.; Collier, D.; Kassotis, C.; Roepke, T. A.; Kim, M. J.; Blanc, E.; Barouki, R.; Bansal, A.; Cave, M. C.; Chatterjee, S.; Choudhury, M.; Gilbertson, M.; Lagadic-Gossmann, D.; Howard, S.; Lind, L.; Tomlinson, C. R.; Vondracek, J.; Heindel, J. J. Obesity I: Overview and molecular and biochemical mechanisms. *Biochem. Pharmacol.* **2022**, *199*, No. 115012.
- (2) Mathieu, P.; Lemieux, I.; Després, J. P. Obesity, inflammation, and cardiovascular risk. *Clin. Pharmacol. Ther.* **2010**, *87* (4), 407–416.
- (3) Stefan, N. Causes, consequences, and treatment of metabolically unhealthy fat distribution. *Lancet Diabetes Endocrinol.* **2020**, *8* (7), 616–627.
- (4) Loomis, A. K.; Kabadi, S.; Preiss, D.; Hyde, C.; Bonato, V.; St Louis, M.; Desai, J.; Gill, J. M. R.; Welsh, P.; Waterworth, D.; Sattar, N. Body Mass Index and Risk of Nonalcoholic Fatty Liver Disease: Two Electronic Health Record Prospective Studies. *J. Clin. Endocrinol. Metab.* **2016**, *101* (3), 945–952.
- (5) Kolotkin, R. L.; Meter, K.; Williams, G. R. Quality of life and obesity. *Obes. Rev.* **2001**, *2* (4), 219–229.
- (6) *About Obesity*. Center for Disease Control 2024. <https://www.cdc.gov/obesity/php/about/index.html#:~:text=Adults%20with%20obesity%20have%20a,affects%20the%20nation's%20military%20readinesshttps://www.cdc.gov/obesity/php/about/index.html#:~:text=Adults%20with%20obesity%20have%20a,affects%20the%20nation's%20military%20readiness>.
- (7) Müller, T. D.; Blüher, M.; Tschöp, M. H.; DiMarchi, R. D. Anti-obesity drug discovery: advances and challenges. *Nat. Rev. Drug Discovery* **2022**, *21* (3), 201–223.
- (8) Arterburn, D. E.; Courcoulas, A. P. Bariatric surgery for obesity and metabolic conditions in adults. *BMJ* **2014**, *349*, g3961.
- (9) Mahapatra, M. K.; Karuppusamy, M.; Sahoo, B. M. Semaglutide, a glucagon like peptide-1 receptor agonist with cardiovascular benefits

for management of type 2 diabetes. *Rev. Endocr. Metab. Disord.* **2022**, *23* (3), 521–539.

(10) Rubino, D.; Abrahamsson, N.; Davies, M.; Hesse, D.; Greenway, F. L.; Jensen, C.; Lingvay, I.; Mosenzon, O.; Rosenstock, J.; Rubio, M. A.; Rudofsky, G.; Tadayon, S.; Wadden, T. A.; Dicker, D. Effect of Continued Weekly Subcutaneous Semaglutide vs Placebo on Weight Loss Maintenance in Adults With Overweight or Obesity: The STEP 4 Randomized Clinical Trial. *JAMA* **2021**, *325* (14), 1414–1425.

(11) Jastreboff, A. M.; Aronne, L. J.; Ahmad, N. N.; Wharton, S.; Connery, L.; Alves, B.; Kiyosue, A.; Zhang, S.; Liu, B.; Bunck, M. C.; Stefanski, A. Tirzepatide Once Weekly for the Treatment of Obesity. *N. Engl. J. Med.* **2022**, *387* (3), 205–216.

(12) Tan, B.; Pan, X.-H.; Chew, H. S. J.; Goh, R. S. J.; Lin, C.; Anand, V. V.; Lee, E. C. Z.; Chan, K. E.; Kong, G.; Ong, C. E. Y.; Chung, H. C.; Young, D. Y.; Chan, M. Y.; Khoo, C. M.; Mehta, A.; Muthiah, M. D.; Nouredin, M.; Ng, C. H.; Chew, N. W. S.; Chin, Y. H. Efficacy and safety of tirzepatide for treatment of overweight or obesity. A systematic review and meta-analysis. *Int. J. Obes.* **2023**, *47* (8), 677–685.

(13) Singh, G.; Krauthamer, M.; Bjalme-Evans, M. Wegovy (semaglutide): a new weight loss drug for chronic weight management. *J. Investig. Med.* **2022**, *70* (1), 5–13.

(14) Bikou, A.; Dermiki-Gkana, F.; Penteris, M.; Constantinides, T. K.; Kontogiorgis, C. A systematic review of the effect of semaglutide on lean mass: insights from clinical trials. *Expert Opin. Pharmacother.* **2024**, *25* (5), 611–619.

(15) Hathaway, J. T.; Shah, M. P.; Hathaway, D. B.; Zekavat, S. M.; Krasniqi, D.; Gittinger, J. W., Jr; Cestari, D.; Mallery, R.; Abbasi, B.; Bouffard, M.; Chwalisz, B. K.; Estrela, T.; Rizzo, J. F., III Risk of Nonarteritic Anterior Ischemic Optic Neuropathy in Patients Prescribed Semaglutide. *JAMA Ophthalmol.* **2024**, *142* (8), 732–739.

(16) Zhou, X.-D.; Wong, V. W.-S.; Zheng, M.-H. Resmetirom and GLP-1 agonists for MASH: complementary rather than exclusive. *npj Gut Liver* **2024**, *1* (1), No. 4.

(17) Kanwal, F.; Neuschwander-Tetri, B. A.; Loomba, R.; Rinella, M. E. Metabolic dysfunction–associated steatotic liver disease: Update and impact of new nomenclature on the American Association for the Study of Liver Diseases practice guidance on nonalcoholic fatty liver disease. *Hepatology* **2024**, *79* (5), 1212–1219, DOI: 10.1097/HEP.0000000000000670.

(18) Perumpail, B. J.; Khan, M. A.; Yoo, E. R.; Cholankeril, G.; Kim, D.; Ahmed, A. Clinical epidemiology and disease burden of nonalcoholic fatty liver disease. *World J. Gastroenterol.* **2017**, *23* (47), 8263–8276.

(19) Rinella, M. E. Nonalcoholic fatty liver disease: a systematic review. *JAMA* **2015**, *313* (22), 2263–2273.

(20) Administration, U. S. F. D. FDA Approves First Treatment for Patients with Liver Scarring Due to Fatty Liver Disease, 2024. <https://www.fda.gov/news-events/press-announcements/fda-approves-first-treatment-patients-liver-scarring-due-fatty-liver-disease>.

(21) Reichman, T. W.; Therapondos, G.; Serrano, M. S.; Seal, J.; Evers-Meltzer, R.; Bohorquez, H.; Cohen, A.; Carmody, I.; Ahmed, E.; Bruce, D.; Loss, G. E.; et al. "Weighing the risk": Obesity and outcomes following liver transplantation. *World J. Hepatol.* **2015**, *7* (11), 1484–1493.

(22) Paklar, N.; Mijic, M.; Filipec-Kanizaj, T. The Outcomes of Liver Transplantation in Severe Metabolic Dysfunction-Associated Steatotic Liver Disease Patients. *Biomedicines* **2023**, *11* (11)3096.

(23) Koliaki, C.; Szendroedi, J.; Kaul, K.; Jelenik, T.; Nowotny, P.; Jankowiak, F.; Herder, C.; Carstensen, M.; Krausch, M.; Knoefel, W. T.; Schlensak, M.; Roden, M. Adaptation of hepatic mitochondrial function in humans with non-alcoholic fatty liver is lost in steatohepatitis. *Cell Metab.* **2015**, *21* (5), 739–746.

(24) Shum, M.; Ngo, J.; Shirihai, O. S.; Liesa, M. Mitochondrial oxidative function in NAFLD: Friend or foe? *Mol. Metab.* **2021**, *50*, No. 101134.

(25) Rector, R. S.; Thyfault, J. P.; Uptergrove, G. M.; Morris, E. M.; Naples, S. P.; Borengasser, S. J.; Mikus, C. R.; Laye, M. J.; Laughlin,

- M. H.; Booth, F. W.; Ibdah, J. A. Mitochondrial dysfunction precedes insulin resistance and hepatic steatosis and contributes to the natural history of non-alcoholic fatty liver disease in an obese rodent model. *J. Hepatol.* **2010**, *52* (5), 727–736.
- (26) Manna, P.; Jain, S. K. Obesity, Oxidative Stress, Adipose Tissue Dysfunction, and the Associated Health Risks: Causes and Therapeutic Strategies. *Metab. Syndr. Relat. Disord.* **2015**, *13* (10), 423–444.
- (27) Enoch, S. J.; Schultz, T. W.; Popova, I. G.; Vasilev, K. G.; Mekenyan, O. G. Development of a Decision Tree for Mitochondrial Dysfunction: Uncoupling of Oxidative Phosphorylation. *Chem. Res. Toxicol.* **2018**, *31* (8), 814–820.
- (28) Farrell, G. C.; van Rooyen, D.; Gan, D.; Chitturi, S. NASH is an Inflammatory Disorder: Pathogenic, Prognostic and Therapeutic Implications. *Gut Liver* **2012**, *6* (2), 149–171.
- (29) Demine, S.; Renard, P.; Arnould, T. Mitochondrial Uncoupling: A Key Controller of Biological Processes in Physiology and Diseases. *Cells* **2019**, *8* (8795).
- (30) El-Yazbi, A. F.; Elrewiny, M. A.; Habib, H. M.; Eid, A. H.; Elzahhar, P. A.; Belal, A. S. F. Thermogenic Modulation of Adipose Depots: A Perspective on Possible Therapeutic Intervention with Early Cardiorenal Complications of Metabolic Impairment. *Mol. Pharmacol.* **2023**, *104* (5), 187.
- (31) Grundlingh, J.; Dargan, P. I.; El-Zanfaly, M.; Wood, D. M. 2,4-dinitrophenol (DNP): a weight loss agent with significant acute toxicity and risk of death. *J. Med. Toxicol.* **2011**, *7* (3), 205–212.
- (32) Geisler, J. G. 2,4 Dinitrophenol as Medicine. *Cells* **2019**, *8* (3280).
- (33) Poole, F. E.; Haining, R. B. Sudden Death from Dinitrophenol Poisoning: Report of a Case with Autopsy. *JAMA* **1934**, *102* (14), 1141–1147.
- (34) Tainter, M. L.; Stockton, A. B.; Cutting, W. C. Use of Dinitrophenol in Obesity and Related Conditions: A Progress Report. *JAMA* **1933**, *101* (19), 1472–1475.
- (35) Childress, E. S.; Alexopoulos, S. J.; Hoehn, K. L.; Santos, W. L. Small Molecule Mitochondrial Uncouplers and Their Therapeutic Potential. *J. Med. Chem.* **2018**, *61* (11), 4641–4655.
- (36) Buckler, K. J.; Vaughan-Jones, R. D. Effects of mitochondrial uncouplers on intracellular calcium, pH and membrane potential in rat carotid body type I cells. *J. Physiol.* **1998**, *513* (Pt 3), 819–833.
- (37) Perry, R. J.; Kim, T.; Zhang, X.-M.; Lee, H.-Y.; Pesta, D.; Popov, V. B.; Zhang, D.; Rahimi, Y.; Jurczak, M. J.; Cline, G. W.; et al. Reversal of hypertriglyceridemia, fatty liver disease, and insulin resistance by a liver-targeted mitochondrial uncoupler. *Cell Metab.* **2013**, *18* (5), 740–748.
- (38) Perry, R. J.; Zhang, D.; Zhang, X. M.; Boyer, J. L.; Shulman, G. I. Controlled-release mitochondrial protonophore reverses diabetes and steatohepatitis in rats. *Science* **2015**, *347* (6227), 1253–1256.
- (39) Wei, G.; Song, X.; Fu, Y.; Gong, T.; Zhang, Q. Sustained-release mitochondrial protonophore reverses nonalcoholic fatty liver disease in rats. *Int. J. Pharm.* **2017**, *530* (1–2), 230–238.
- (40) Goedeke, L.; Peng, L.; Montalvo-Romeral, V.; Butrico, G. M.; Dufour, S.; Zhang, X. M.; Perry, R. J.; Cline, G. W.; Kievit, P.; Chng, K.; Petersen, K. F.; Shulman, G. I. Controlled-release mitochondrial protonophore (CRMP) reverses dyslipidemia and hepatic steatosis in dysmetabolic nonhuman primates. *Sci. Transl. Med.* **2019**, *11* (512), No. eaay0284, DOI: 10.1126/scitranslmed.aay0284.
- (41) HKhan, S. Novel Phenyl Derivatives. USA WO2018/129258A1, 2018.
- (42) A 61-day Randomized, Double Blind, Placebo-controlled Trial to Assess the Safety and Efficacy of Three Doses of HU6 in Subjects With Elevated Liver Fat and High Body Mass Index (28 to 45 kg/m²). <https://clinicaltrials.gov/study/NCT04874233>.
- (43) Foutz, M., In *BioRender*, BioRender.com/c16u063, Ed. 2024.
- (44) Kenwood, B. M.; Weaver, J. L.; Bajwa, A.; Poon, I. K.; Byrne, F. L.; Murrow, B. A.; Calderone, J. A.; Huang, L.; Divakaruni, A. S.; Tomsig, J. L.; et al. Identification of a novel mitochondrial uncoupler that does not depolarize the plasma membrane. *Mol. Metab.* **2014**, *3* (2), 114–123.
- (45) Xiong, G.; Zhang, K.; Ma, Y.; Song, Y.; Zhang, W.; Qi, T.; Qiu, H.; Shi, J.; Kan, C.; Zhang, J.; Sun, X. BAM15 as a mitochondrial uncoupler: a promising therapeutic agent for diverse diseases. *Front. Endocrinol.* **2023**, *14*, No. 1252141.
- (46) Shrestha, R.; Johnson, E.; Byrne, F. L. Exploring the therapeutic potential of mitochondrial uncouplers in cancer. *Mol. Metab.* **2021**, *51*, No. 101222.
- (47) Salamoun, J. M.; Garcia, C. J.; Hargett, S. R.; Murray, J. H.; Chen, S.-Y.; Beretta, M.; Alexopoulos, S. J.; Shah, D. P.; Olzomer, E. M.; Tucker, S. P.; Hoehn, K. L.; Santos, W. L. 6-Amino[1,2,5]-oxadiazolo[3,4-b]pyrazin-5-ol Derivatives as Efficacious Mitochondrial Uncouplers in STAM Mouse Model of Nonalcoholic Steatohepatitis. *J. Med. Chem.* **2020**, *63* (11), 6203–6224.
- (48) Murray, J. H.; Burgio, A. L.; Beretta, M.; Hargett, S. R.; Harris, T. E.; Olzomer, E.; Grams, R. J.; Garcia, C. J.; Li, C.; Salamoun, J. M.; Hoehn, K. L.; Santos, W. L. Oxadiazolopyridine Derivatives as Efficacious Mitochondrial Uncouplers in the Prevention of Diet-Induced Obesity. *J. Med. Chem.* **2023**, *66* (6), 3876–3895.
- (49) Oligschlaeger, Y.; Shiri-Sverdlov, R. NAFLD Preclinical Models: More than a Handful, Less of a Concern? *Biomedicines* **2020**, *8* (228).
- (50) Vacca, M.; Kamzolas, I.; Harder, L. M.; Oakley, F.; Trautwein, C.; Hatting, M.; Ross, T.; Bernardo, B.; Oldenburger, A.; Hjuler, S. T.; Ksiazek, I.; Lindén, D.; Schuppan, D.; Rodriguez-Cuenca, S.; Tonini, M. M.; Castañeda, T. R.; Kannt, A.; Rodrigues, C. M. P.; Cockell, S.; Govaere, O.; Daly, A. K.; Allison, M.; Honnens de Lichtenberg, K.; Kim, Y. O.; Lindblom, A.; Oldham, S.; Andréasson, A.-C.; Schlerman, F.; Marioneaux, J.; Sanyal, A.; Afonso, M. B.; Younes, R.; Amano, Y.; Friedman, S. L.; Wang, S.; Bhattacharya, D.; Simon, E.; Paradis, V.; Burt, A.; Grypari, I. M.; Davies, S.; Driessen, A.; Yashiro, H.; Pors, S.; Worm Andersen, M.; Feigh, M.; Yunis, C.; Bedossa, P.; Stewart, M.; Cater, H. L.; Wells, S.; Schattenberg, J. M.; Anstee, Q. M.; Anstee, Q. M.; Daly, A. K.; Cockell, S.; Tiniakos, D.; Bedossa, P.; Burt, A.; Oakley, F.; Cordell, H. J.; Day, C. P.; Wonders, K.; Missier, P.; McTeer, M.; Vale, L.; Oluboyede, Y.; Breckons, M.; Boyle, J.; Bossuyt, P. M.; Zafarmand, H.; Vali, Y.; Lee, J.; Nieuwdorp, M.; Holleboom, A. G.; Angelakis, A.; Verheij, J.; Ratziu, V.; Clément, K.; Patino-Navarrete, R.; Pais, R.; Paradis, V.; Schuppan, D.; Schattenberg, J. M.; Surabattula, R.; Myneni, S.; Kim, Y. O.; Straub, B. K.; Vidal-Puig, A.; Vacca, M.; Rodrigues-Cuenca, S.; Allison, M.; Kamzolas, I.; Petsalaki, E.; Campbell, M.; Lelliott, C. J.; Davies, S.; Orešič, M.; Hyötyläinen, T.; McGlinchey, A.; Mato, J. M.; Millet, O.; Dufour, J.-F.; Berzigotti, A.; Masoodi, M.; Lange, N. F.; Pavlides, M.; Harrison, S.; Neubauer, S.; Cobbold, J.; Mozes, F.; Akhtar, S.; Olodo-Atitebi, S.; Banerjee, R.; Shumbayawonda, E.; Dennis, A.; Andersson, A.; Wigley, I.; Romero-Gómez, M.; Gómez-González, E.; Ampuero, J.; Castell, J.; Gallego-Durán, R.; Fernández-Lizaranzu, I.; Montero-Vallejo, R.; Karsdal, M.; Rasmussen, D. G. K.; Leeming, D. J.; Sinisi, A.; Musa, K.; Sandt, E.; Tonini, M. M.; Bugianesi, E.; Rosso, C.; Armandi, A.; Marra, F.; Gastaldelli, A.; Svegliati, G.; Boursier, J.; Franque, S.; Vonghia, L.; Verrijken, A.; Dirinck, E.; Driessen, A.; Ekstedt, M.; Kechagias, S.; Yki-Järvinen, H.; Porthan, K.; Arola, J.; van Mil, S.; Papatheodoridis, G.; Cortez-Pinto, H.; Silva, A. P.; Rodrigues, C. M. P.; Valenti, L.; Pelusi, S.; Petta, S.; Pennisi, G.; Miele, L.; Liguori, A.; Geier, A.; Rau, M.; Trautwein, C.; Reißing, J.; Aithal, G. P.; Francis, S.; Palaniyappan, N.; Bradley, C.; Hockings, P.; Schneider, M.; Newsome, P. N.; Hübscher, S.; Wenn, D.; Magnanensi, J.; Trylesinski, A.; Mayo, R.; Alonso, C.; Duffin, K.; Perfield, J. W.; Chen, Y.; Hartman, M. L.; Yunis, C.; Miller, M.; Chen, Y.; McLeod, E. J.; Ross, T.; Bernardo, B.; Schölch, C.; Ertle, J.; Younes, R.; Coxson, H.; Simon, E.; Gogain, J.; Ostroff, R.; Alexander, L.; Biegel, H.; Kjær, M. S.; Harder, L. M.; Al-Sari, N.; Veidal, S. S.; Oldenburger, A.; Ellegaard, J.; Balp, M.-M.; Jennings, L.; Martic, M.; Löffler, J.; Applegate, D.; Torstenson, R.; Lindén, D.; Fournier-Poizat, C.; Llorca, A.; Kalutkiewicz, M.; Pepin, K.; Ehman, R.; Horan, G.; Ho, G.; Tai, D.; Chng, E.; Xiao, T.; Patterson, S. D.; Billin, A.; Doward, L.; Twiss, J.; Thakker, P.; Derdak, Z.; Yashiro, H.; Landgren, H.; Lackner, C.; Gouw, A.; Hytiroglou, P.; Govaere, O.; Brass, C.; Tiniakos, D.; Perfield, J. W.; Petsalaki, E.; Davidsen, P.; Vidal-Puig, A. An unbiased

ranking of murine dietary models based on their proximity to human metabolic dysfunction-associated steatotic liver disease (MASLD). *Nat. Metab.* **2024**, *6* (6), 1178–1196.